THESIS ON NATURAL AND EXACT SCIENCES B61

Sol-Gel Deposition of Titanium Dioxide Films

ILONA OJA AÇIK

TALLINN 2007

TALLINN UNIVERSITY OF TECHNOLOGY
Faculty of Chemistry and Materials Technology
Department of Materials Science
Chair of Semiconductor Materials Technology

Dissertation was accepted for defence of the degree of Doctor of Philosophy in Natural and Exact Sciences on April 3, 2007.

Supervisor: Research Professor Malle Krunks, Department of Materials Science, Tallinn University of Technology

Opponents: Professor Markku Leskelä, University of Helsinki, Finland
Dr. Ilmo Sildos, University of Tartu, Estonia

Defence: June 14, 2007, at 14.00
Lecture hall: VII-226
Tallinn University of Technology, Ehitajate tee 5, Tallinn

Declaration: Hereby I declare that this doctoral thesis, my original investigation and achievement, submitted for the doctoral degree at Tallinn University of Technology has not been submitted for any degree or examination.

Ilona Oja Açik

ISSN 1406-4723
ISBN 978-9985-59-702-6

LOODUS- JA TÄPPISTEADUSED B61

Titaandioksiidi kiled sool-geeli meetodil

ILONA OJA AÇIK

TALLINN 2007

TALLINNA TEHNIKAÜLIKOOL
Keemia-ja materjalitehnoloogia teaduskond
Materjaliteaduse instituut
Pooljuhtmaterjalide tehnoloogia õppetool

Doktoritöö on vastu võetud avalikuks kaitsmiseks filosoofiadoktori kraadi (keemia- ja materjalitehnoloogia erialal) taotlemiseks 3. aprillil 2007

Juhendaja:	Uurija-Professor Malle Krunks, Materjaliteaduse Instituut, Tallinna Tehnikaülikool
Oponendid:	Professor Markku Leskelä, Helsingi Ülikool Dr. Ilmo Sildos, Tartu Ülikool
Avalik kaitsmine:	14. juuni 2007, kell 14.00 Ruum: VII-226 Tallinna Tehnikaülikool, Ehitajate tee 5, Tallinn

Deklaratsioon: Deklareerin, et käesolev doktoritöö, mis on minu iseseisva töö tulemus, on esitatud Tallinna Tehnikaülikooli doktorikraadi taotlemiseks ja selle alusel ei ole varem taotletud akadeemilist kraadi

Ilona Oja Açik

Table of contents

LIST OF PUBLICATIONS

The present doctoral thesis is based on the following papers, which are referred to in the text by their Roman numerals **I-VI**.

I M. Krunks, **I. Oja**, K. Tõnsuaadu, M. Es-Souni, M. Gruselle, L. Niinistö, Thermoanalytical study of acetylacetonate-modified titanium(IV) isopropoxide as a precursor for TiO_2 films, *Journal of Thermal Analysis and Calorimetry*, 80 (2005) 483–488.

II **I.Oja Açik**, J. Madarász, M. Krunks, K. Tõnsuaadu, D. Janke, G. Pokol, L. Niinistö, Thermoanalytical studies of titanium(IV) acetylacetonate xerogels with emphasis on evolved gas analysis, *Journal of Thermal Analysis and Calorimetry*, 88 (2007) 2, in press (DOI:10.1007/s10973-006-8064-6).

III **I. Oja**, A. Mere, M. Krunks, C-H. Solterbeck, M. Es-Souni, Properties of TiO_2 films prepared by the spray pyrolysis method, *Solid State Phenomena*, 99-100 (2004) 259–262.

IV **I. Oja**, A. Mere, M. Krunks, R. Nisumaa, C-H. Solterbeck, M. Es-Souni, Structural and electrical characterization of TiO_2 films grown by spray pyrolysis, *Thin Solid Films,* 515 (2006) 674–677.

V J. Sabataityté, **I. Oja**, F. Lenzmann, O. Volobujeva, M. Krunks, Characterization of nanoporous TiO_2 films prepared by sol-gel method. *Comptes Rendus Chimie*, 9 (2006) 708–712.

VI **I. Oja**, A. Belaidi, L. Dloczik, M-Ch. Lux-Steiner, Th. Dittrich, Photoelectrical properties of $In(OH)_xS_y$/PbS(O) structures deposited by SILAR on TiO_2, *Semiconductor Science and Technology*, 21 (2006) 520–526.

In the appendix A, copies of these papers have been included.

Author's own contribution

The contribution by the author to the papers included in the thesis is as follows:

I Gel synthesis, characterization by FTIR and analysis; thermal analysis of dried gel powders (TG/DTA/EGA-FTIR measurements, characterisation of solid intermediates and final products by FTIR), analysis of results and minor part of writing.

II Gels synthesis, characterization by FTIR and analysis; dried gel powders characterization (TG/DTA/EGA-FTIR, TG/DTA/EGA-MS measurements), analysis of results and major part of writing.

III Sol preparation, films deposition, films characterization (FTIR, ellipsometry, impedance spectroscopy and electrometric measurements), analysis of results and major part of writing.

IV Sol preparation, films deposition, films characterization (Raman, ellipsometry and impedance spectroscopy measurements), analysis of results and major part of writing.

V Part of the experimental work (sol preparation, films deposition), films characterization (FTIR), analysis of results, major part of writing.

VI Solar cell preparation, layers characterization by Kelvin probe and SPV, Current-Voltage and QE measurements of solar cells, part of the analysis and minor part of writing.

List of abbreviations and symbols

acacH	acetylacetone
acac	acetylacetonate
AC	Alternating Current
AFM	Atomic Force Microscopy
ALD	Atomic Layer Deposition
Bu^n	butyl
BuOH	butanol
CVD	Chemical Vapour Deposition
CSP	Chemical Spray Pyrolysis
DB	Doctor Blading
DEA	diethanolamine
DTA	Differential Thermal Analysis
DTG	Differential Thermogravimetry
E_A	activation energy of conductivity
EGA	Evolved Gas Analysis
Et	ethyl
eta	extremely thin absorber
EtOH	ethanol
FF	Fill Factor
FTIR	Fourier Transform Infrared Spectroscopy
FWHM	Full Width at Half Maximum
I-V	Current-Voltage
IR	Infrared
LP-MOCVD	Low Pressure Metal Organic Chemical Vapor Deposition
Me	methyl
MeOH	methanol
MBE	Molecular Beam Epitaxy
MOCVD	Metal Organic Chemical Vapor Deposition
MOE	methoxyethanol
MS	Mass Spectrometer
NIST	National Institute of Standards and Technology
nm	nanometre
OR	alkoxy group
JCPDS-PDF	Joint Committee on Powder Diffraction Standards- Powder Diffraction File
PEDOT:PSS	Poly(3,4-ethylenedioxythiophene) poly(styrenesulfonate)
PEG	polyethylene glycol
PEG600	polyethylene glycol, molecular weight 600 g/mol
PVD	Physical Vapour Deposition
QE	Quantum Efficiency
RIR	Reference Intensity Ratio
rpm	rotations per minute

rms	root mean square
RT	Room Temperature
SC	Solar Cell
SEM	Scanning Electron Microscopy
SILAR	Successive Ionic Layer Adsorption and Reaction
TA	Thermal Analysis
T_{AN}	annealing temperature
TG	Thermogravimetric Analysis
Tiacac	Titanium acetylacetonate
T_S	substrate temperature
TTBU	titanium (IV) tetrabutoxide
TTET	titanium (IV) tetraethoxide
TTIP	titanium (IV) tetraisopropoxide
XRD	X-Ray Diffraction
2-MOE	2-methoxyethanol
2-PrOH	2-propanol
ε	effective dielectric constant
μm	micrometre
σ	conductivity
j_{SC}	short circuit current density
V_{OC}	open circuit voltage
η	efficiency of solar cell

INTRODUCTION

TiO_2 films, prepared by a variety of deposition techniques, have attracted wide interest as dielectric, photocatalytic and photovoltaic materials [1-3]. The sol-gel process allows the preparation of homogeneous materials with controlled structure-property characteristics by chemically modifying the precursor systems [4]. Sol-gel based film processing routes such as dip-coating, spray pyrolysis and spin-coating are usually applied because they are versatile and cost-effective. A better understanding of the thermal behaviour of gels formed in a sol-gel process would enable to optimize the post-deposition annealing or deposition conditions and thus improve the properties of TiO_2 films.

The present thesis "Sol-Gel Deposition of Titanium Dioxide Films" is devoted to TiO_2 films, deposited by the cost-effective, non-vacuum sol-gel process. In this study we focused on the formation of TiO_2 as well as on the development of flat and porous TiO_2 films. As an example of applications, eta-solar cell based on TiO_2 window layer was prepared and characterized.

This thesis is divided into four Chapters. Following the introduction, a literature summary is briefly given in Chapter 1. In Chapter 2, the preparation of materials and the experimental methods are reviewed. Chapter 3 is divided into four different parts. The first part describes the formation of TiO_2 from dried titania gels monitored by thermal analysis coupled with evolved gas analysis by MS and FTIR. The second part gives an overview of the sol-gel derived TiO_2 films grown by spray pyrolysis. The morphological, optical, structural and electrical properties of TiO_2 films as a function of substrate and annealing temperatures are given in this part of the work. The third part introduces the sprayed and spin-coated porous TiO_2 films by characterizing their morphology and structural properties. The fourth part describes the preparation of an eta- solar cell structure where sol-gel derived TiO_2 window layer is used. The possible ways for optimization of this type of solar cell are studied. Finally, in Chapter 4 the summary of the main results is given.

The work is financially supported by Estonian Science Foundation grants 5612 and 6954, German Federal Ministry of Education and Research (BMBF) under the WTZ project EST 02/001, European Commission RTN-project HRNP-CT-2000-00101, EU FP5 project ENK6-CT-2002-80664, Deutsche Bundesstiftung Umwelt (DBU) and Estonian Doctoral School of Materials Science and Materials Technology (MMTDK). This doctoral thesis is based on 6 published papers.

1 LITERATURE REVIEW AND AIM OF THE WORK

1.1 Titanium dioxide

Titanium dioxide (TiO_2) belongs to the family of transition metal oxides and is also occurring as a mineral in the nature [5]. TiO_2 has received a great deal of attention due to its chemical stability, non-toxicity, low cost and other advantageous properties. The physical properties of TiO_2 make it suitable for thin film applications. Because of their good transmittance in the visible region, high refractive index and chemical stability, TiO_2 films have found wide application for various optical coatings [6, 7]. The high dielectric constant ε of TiO_2 (the largest ε among simple metal oxides) opens prospects for the use of TiO_2 thin films in microelectronic devices [8, 9], *e.g.* in capacitors or as a gate dielectric in metal-dielectric-semiconductor devices. During the last decade, TiO_2 films have been suggested as photoanodes in the process of photoelectrolysis of water (in solar energy conversion systems) [10], photocatalysis [5] and as a window layer in photovoltaic solar cells; *e.g.* so-called Grätzel cell [11] and eta-solar cell [12]. TiO_2 is also successfully used as gas sensor [13], biomaterial [14] and promoter in catalytic reactions [15].

1.1.1 Material properties

TiO_2 occurs in three crystalline modifications- brookite (orthorhombic), anatase (tetragonal) and rutile (tetragonal) all containing the TiO_6 octahedra (Fig. 1.1). Anatase and brookite irreversibly convert to rutile at temperatures approximately 800 °C [16]. The band gap of TiO_2 is determined by the crystal modification and in the case of thin films the reported values are: 3.5 eV for amorphous films, 3.2 eV for crystalline films in the anatase phase and 3.0 eV for crystalline films in the rutile phase [5, 9].

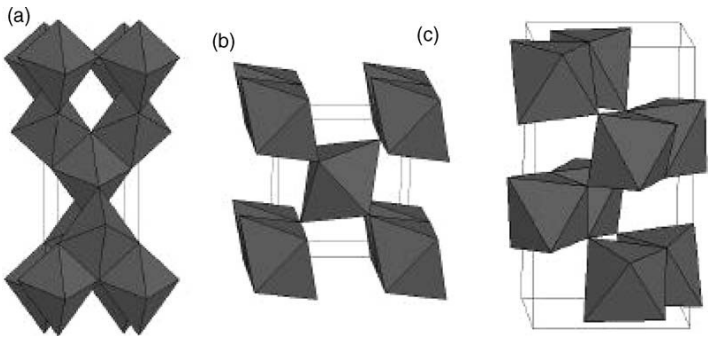

Figure 1.1. Crystal structures of anatase (a), rutile (b), and brookite (c) [5].

TiO_2 can be prepared in the form of powders, crystals or thin films. The most commonly used solution routes in the synthesis of TiO_2 films are [5]: solvent routes such as sol-gel spin-coating and spray pyrolysis; electrochemical synthesis, and vapour-phase deposition methods such as chemical vapour deposition (CVD), physical vapour deposition (PVD), sputtering, molecular beam epitaxy (MBE) and atomic layer deposition (ALD) [17-19].

1.2 Sol-gel process

Sol-gel processing has been known for a long time; the first silica gels were made in 1845 by M. Ebelman at the "Manufacture de Ceramiques de Sevres" in Sevres, France [20].
Basically, starting from molecular precursors, an oxide network is obtained *via* inorganic polymerization reactions. These reactions occur in solutions and the term "sol-gel processing" is often used in a broad sense to describe the synthesis of inorganic oxides by methods of "wet chemistry" [21].
The advantages of the sol-gel process reside in its low-cost, the high purity of the metal alkoxide precursors, the homogeneity of the components at the molecular level, the low processing temperature, possibility to use different substrate materials, good control over the material properties for a single layer up to heterostructures, control of porosity by using appropriate heat treatment and firing times [20]. The greatest limitations of the sol-gel processing are its long processing times (compared with sputtering), health hazard of some organic solutions, large shrinkage, development of stress leading to fragmentation, residual fine pores and residual hydroxyl [20].

1.2.1 Basic overview of the sol-gel chemistry

Several overviews of the sol-gel processing have been published in [20-24].
Briefly, sol-gel processing involves the use of molecular precursors, mainly alkoxides, as starting materials. A macromolecular oxide network is obtained through hydrolysis and condensation. These reactions are usually written as follows [24]:

$$M(OR)_n + H_2O \rightarrow M(OR)_{n-1}(OH) + ROH \text{ (hydrolysis)} \quad (1.1)$$

$$M(OR)_n + M(OR)_{n-1}(OH) \rightarrow M_2O(OR)_{2n-2} + ROH \text{ (condensation)}, \quad (1.2)$$

where OR is an alkoxide group.
The chemical reactivity of metal atom toward hydrolysis mainly depends on the electronegativity of the metal atom and its ability to increase its coordination number. As a general rule, the coordination number increases when going down in the periodic table. Coordination expansion is a general tendency of transition metal alkoxides $M(OR)_z$. It may occur *via* oligomerization. The molecular complexity of

metal alkoxides depends on concentration, temperature, nature of the solvent, oxidation state of the metal atom or the steric hindrance of alkoxide groups. The chemical reactivity of a given metal alkoxide $M(OR)_z$ decreases when its molecular complexity increases. This is why $Ti(OBu^n)_4$ (TTBU) is often used as a precursor for TiO_2 films. The Bu^n group is the largest one of these alkoxides that does not prevent oligomerization. Oligomerization can be prevented by solvation in a polar solvent or by steric hindrance with bulky alkoxy ligands. Titanium ethoxide, for instance, gives $(Ti(OEt)_4)_n$ (TTET) oligomers ($n \approx 4$) whereas titanium iso-propoxide $Ti(OPr^i)_4$ (TTIP) remains monomeric [7].
One of the main drawbacks (which can also be an advantage) of transition metal alkoxides is their high reactivity with water. In order to retard hydrolysis and condensation rates chemical additives are almost always used. Moreover they can also improve the sol-gel process to obtain better materials. Such additives can be solvents *e.g.* 2-methoxyetehanol (2-MOE) [24-26], acids *e.g.* HCl [27, 28] or basic catalysts *e.g.* NaOH [29], stabilizing agents *e.g.* acetylacetone (acacH) [24], acetic acid [24], or drying control chemical additives *e.g.* formide [27]. In most cases they are nucleophilic XOH molecules that react with the alkoxide giving rise to a new molecular precursor [24]:

$$M(OR)_n + x\ XOH = M(OR)_{n-x}(OX)_x + x\ ROH. \qquad (1.3)$$

Summarizing, in the case of metal alkoxide precursors, the main sol-gel process parameters are: the nature of the metal; the nature of the alkoxide species bonded to the metal (steric hindrance, polarity, *etc*.); the water to precursor molar ratio used in the hydrolysis; the use of a catalyst (for hydrolysis and condensation reactions); the use of a solvent in order to get a homogeneous initial solution and to dilute the reactants; the use of ligands in order to modify (usually to quench) the intrinsic reactivity of the precursor [21-23].

1.3 Stabilized Ti-alkoxides and their thermal behaviour

Thermoanalytical (TA) studies of sol-gel derived precursors for TiO_2 have grown up from the necessity to find the proper temperature profiles for the film deposition. As the film growth by spray pyrolysis and spin coating methods is a thermal process then the film formation can be controlled by the film deposition and/or annealing temperatures. Moreover, it has been reported that crystal structure of dip-coated TiO_2 films can be controlled by the TTIP:acacH molar ratio in the precursor solution [30].
Our first results on sol-gel derived TiO_2 films have been published in 2004 [31]. We have deposited flat TiO_2 films by spin-coating technique using the sol which consists of TTIP:acacH:2-MOE in the molar ratio of 1:1:10 [32]. Based on the fact that no TA studies dealing with this precursor system have been published and in the interest of finding the proper temperature profile for TiO_2 film formation we have conducted TA studies (TG/DTA/DTG, coupled with EGA-FTIR and EGA-

MS) to characterize our precursor system. In our studies [I, II] we have characterized sol-gel derived dried TiO_2 gel powders using the TTIP:acacH in molar ratio of 1 or 2 in the precursor solution.
Considering our TA studies, this part of the literature summary focuses; firstly, on the Ti-alkoxide complexes with acacH, secondly, on the possible interchange reaction of Ti-alkoxides with 2-MOE and finally on the TA studies of sol-gel derived dried TiO_2-gel powders.

1.3.1 Ti-complexes stabilized by acetylacetone

Acetylacetone (acacH) has often been used in sol-gel processing as a chemical additive to reduce the reactivity of metal alkoxide precursors, *viz.* $Ti(OPr^i)_4$ [26, 33, 34], $Ti(OBu^n)_4$ [23], $Ti(OEt)_4$ [33]. The reaction of $Ti(OPr^i)_4$ with acacH has been studied in detail by many researchers using FTIR and NMR techniques [33, 34]. It is known that only dimeric $[Ti(OR)_3(acac)]_2$ or monomeric *cis*-$Ti(OR)_2(acac)_2$ can be formed when $Ti(OR)_4$ reacts with acacH in a 1:1 or 1:2 molar ratio, respectively [23]. The structures of both types of compounds are schematically depicted in Fig. 1.2. Sedlar and Sayer [26] have found that when the acacH content in TTIP:acacH exceeds 2, free acacH appears, indicated by bands at 1727 and 1709 cm^{-1} in IR spectrum.

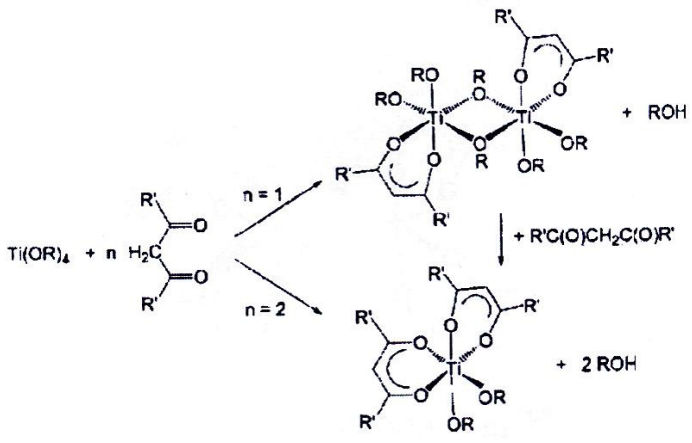

Figure 1.2. Scheme of the $[Ti(OR)_3(acac)]_2$ and *cis*-$Ti(OR)_2(acac)_2$ formation [23].

1.3.2 Interchange reaction of Ti-alkoxides with 2-methoxyethanol

Alkoxide reactivity can also be easily modified by changing the solvent. Metal alkoxides react with a variety of alcohols to create the following type of equilibrium [24]:

$$M(OR)_n + x\ R'OH \leftrightarrow M(OR)_{n-x}(OR')_x + x\ ROH, \qquad (1.4)$$

where OR is an alkoxy group in metal alkoxides and OR' an alkoxy group in alcohols.
In general, the interchange is faciliated when the steric hindrance of the alkoxy group decreases: MeOH> EtOH> 2-PrOH>BuOH [24].
2-methoxyethanol (2-MOE) is the prevailing solvent in sol-gel processing and it is used as a (co-)solvent in sol-gel reactions because it is known to retard the reactivity of metal alkoxides. This is due to alkoxide exchange reactions, i.e., OR groups are exchanged for OR' groups, *e.g.* OCH_2CH_2OMe groups [23, 25, 26]. The results of NMR and FTIR studies on the TTIP reacting with 2-MOE as well as $Ti(OMOE)_4$ in MOE with acacH have been reported by Sedlar and Sayer [26]. These authors have also pointed out that the $Ti(OMOE)_4$ with acetylacetone (TTIP:acacH in equimolar ratio) does not necessarily lead to Ti mono(acetylacetonate) but depends on the mixing procedure [26]. Pathak *et al.* [25] have found that *cis*-$Ti(OR)_2(acac)_2$ reactions with ($R'OCH_2CH_2OH$) (R'=Me, Et, Bu) in 1:1 and 1:2 molar ratios in refluxing benzene under anhydrous conditions yield $[(acac)_2Ti(OR)_{2-n}(OCH_2CH_2OR')_n]$ (n= 1 or 2) complexes.

1.3.3 Thermal behaviour of dried TiO_2-gel powders

Several authors have monitored the TiO_2 film formation with the help of thermal analysis [35-39] in an attempt to find the proper annealing profiles for the film deposition. TA studies of sol-gel derived dried TiO_2-gel powders are briefly described below.
Campostrini *et al.* have conducted several TA studies (by means of coupled thermogravimetric, gas chromatographic and mass spectrometric measurements) of sol-gel derived dried TiO_2-gel powders. In their studies hydrolysed TTIP, under strong acid catalytic conditions, is modified by various stabilizers such as formic [28], oxalic [40] or acetic acid [41] and, also as a comparison, without a chelating agent [42]. Generally, they detected the most abundant release of organic fraction in the temperature range of 100-300 °C. In contrast, for the TiO_2 powders modified by acetic acid ligand the decomposition of organic fraction was completed only above 400 °C. Moreover, they found that the heat treatment temperatures, needed to obtain crystalline TiO_2-anatase phase, vary with organic-modifier at temperatures as high as 415 °C for the formic acid, 430 °C for the acetic acid and 525 °C for the oxalic acid modified gels are needed.
Deshmukh *et al.* [38] have found that thermal decomposition of commercial Tiacac powder, used as a TiO_2 precursor material, consists of five mass loss steps. The weight loss starts at 165 °C showing the most rapid weight loss in the temperature range between 200 and 250 °C. They attributed the weight losses to the decomposition of acetate groups, explosion of gases and crystallization process. The decomposition of Tiacac is completed at 490 °C. Guo *et al.* have published the thermal analysis behaviour of dried TiO_2-gel powders obtained from the precursor sol containing TTIP- H_2O -HCl- PEG (polyethylene glycol) [35]. They found that the xerogels studied displayed three-step weight loss profile. For the PEG-added

xerogels, the second weight loss ranging from 200 and 300 °C is attributed to the expulsion of organics, though whole PEG or organic residues were eliminated before 400 °C. Verma *et al.* have compared the thermal decomposition behaviour of acetic acid stabilized TTIP in EtOH in the presence of diethanolamine (DEA) and acacH [39]. They found that the amorphous to crystalline anatase phase transformation occurs at 323 °C and 561 °C in the presence of DEA and acacH, respectively.
The literature results indicate that the most abundant release of organic fraction takes place in the temperature range of 100-400 °C and the heat treatment temperature, needed to obtain the crystalline TiO_2-anatase phase, depends on the modifier and generally remains between 400 and 500 °C.
It can be concluded that among several surveys on the TA behaviour of dried TiO_2-gel powders [35-42], no TA studies, to our knowledge, on the precursor system containing TTIP, acacH and 2-MOE have been reported.

1.4 TiO_2 films by sol-gel method

Sol-gel derived flat and porous TiO_2 films have been deposited by spin-coating [31, 32, 35, 39], spray pyrolysis (for example, see ref. 38) and dip-coating techniques (for example, see ref. 36).
In the present study spin-coating and spray pyrolysis techniques are used to deposit flat and porous TiO_2 films. Hence this part of the literature survey focuses on flat and porous TO_2 films deposited by spin-coating and spray pyrolysis techniques.

1.4.1 Spray pyrolysis deposition of flat and porous TiO_2 films

Spray pyrolysis technique

Comprehensive overviews of the chemical spray pyrolysis (CSP) technique are given in [43-45]. Shortly, in the chemical spray pyrolysis process, a precursor solution is pulverized with the help of carrier gas onto the preheated substrates. In all spray processes, the significant variables are: substrate temperature, ambient atmosphere, carrier gas and its flow rate; nozzle-to-substrate distance; droplet size; solution concentration and quantity; solution flow rate; substrate motion, *etc*. CSP is a convenient, low-cost, and rapid method for deposition of large-area thin films, which has been used for a long time. Spray pyrolysis has several advantages, including control of the layer thickness, surface morphology and ease of scale-up. Because the film formation in CSP is carried out in air by a simple apparatus, the technique is one of the most attractive film preparation methods.

Flat and porous TiO_2 films by spray pyrolysis

According to literature, TiO_2 films have been deposited by spray pyrolysis usually from alcohol based precursor solutions (EtOH, MeOH, 2-PrOH, 2-BuOH) [38, 46-

54] although occasionally aqueous hydrogen peroxide solutions have been employed as well [55- 57]. Commonly used Ti-sources for TiO_2 film preparation by spray pyrolysis are Tiacac [38, 46, 49, 51] as well as $TiCl_3$ [52], $TiCl_4$ [53], TTIP [47, 50, 54, 58] and Ti metal powder [56, 57]. It must be mentioned that the chemical composition of the used Ti-precursor "titanium acetylacetonate" ("Tiacac") is not precisely determined in the cited papers [38, 46, 51]; except for papers where the di-isopropoxy titanium bis(acetylacetonate) [54] and $TiO[C_5H_7O_2]_2$ [49] are specifically mentioned. Thus, in this study the unidentified Tiacac precursor is indicated as "Tiacac". Several authors have employed acacH as a stabilizer in order to prevent precipitate formation in spraying solution. Usually the deposition is performed in air, but some attempts have also been made to deposit films in an inert atmosphere [58]. A summary on the growth of flat spray deposited TiO_2 films is given in Table 1.1.

Table 1.1. Summary on the deposition of flat TiO_2 films by spray pyrolysis

Precursors	**Deposition parameters**	**T_{AN}, °C**	**Characterization methods**	**Ref.**
"Tiacac" (commercial)+ MeOH	T_S= 200-500 °C cg- air	650-950	XRD, IR, ellipsometry, C-V, AFM, conductivity	[46]
TTIP+alcohol	T_S= 250-500 °C cg- O_2	650-750	XRD, SEM, AFM, UV-VIS	[47]
"Tiacac" (commercial) +MeOH	T_S= 350-450 °C cg-air	500	DTA, XRD, AFM, resistivity	[38]
TTIP+EtOH	T_S= 100-220 °C cg- not presented	400-1100	XRD, EDX, SEM, FTIR	[50]
TTIP+acacH+ 2-PrOH	T_S= 400-450 °C cg- air	500	(XRD), SEM	[54]

cg- carrier gas

Spray pyrolysis deposition have been performed at substrate temperatures between 200 and 500 °C followed by annealing at higher temperatures (600 up to 950 °C) to promote the formation of desired crystalline phase. Crystalline TiO_2-anatase films have been obtained in the substrate temperature range of 300-500 °C [38, 46-50, 53-57], whereas the formation of crystalline TiO_2-rutile phase takes place after further annealing around 800 °C [46, 47, 55]. Castaneda *et al.* [46] have observed, that the thickness of spray deposited TiO_2 films does not show the trend normally observed for films deposited by spray pyrolysis technique, where the thickness of the deposited films decreases as the substrate temperature increases.

It is found by many authors that substrate temperature has an effect on the film structural properties (flat *vs.* porous), leading to the formation of TiO_2 films with higher surface roughness at higher substrates temperatures [55, 57]. It is shown, that the surface morphology and grain size of the sprayed TiO_2 film can be controlled by changing the solvent species such as EtOH, 2-PrOH, BuOH in the

source solution [51, 53]. Optical band gap value of sprayed TiO_2 films are reported for crystalline anatase films as 3.0-3.4 eV [46, 49, 50, 55] and for crystalline rutile films as 3.4 eV [38].
Electrical properties of sprayed TiO_2 films are occasionally investigated, and the reported electrical conductivity values lie between $1 \cdot 10^{-8}$ and $1 \cdot 10^{-12}$ $\Omega^{-1} \cdot cm^{-1}$ [38, 46, 55, 58]. An increase in conductivity by 2-3 orders of magnitude is obtained, for example, in the case of Nb, Li doped or vacuum annealed sprayed TiO_2 films [55, 58].

1.4.2 Spin-coating deposition of flat and porous TiO_2 films

Spin-coating technique

Spin-coating is a method for deposition of thin uniform films onto the substrates. The process is divided into four stages; the first three stages are sequential, while the fourth normally proceeds throughout the coating process [22]. In the first stage (deposition stage) a liquid is delivered onto the substrate, which is at rest or spinning slowly. In the second stage (spin-up stage) the substrate is accelerated up to its final, desired, rotation speed. In the third stage (spin-off stage) the substrate is spinning at a constant rate and fluid viscous forces determine fluid thinning behaviour. The forth stage (evaporation stage) involves spinning of the substrate at a constant rate and solvent evaporation dominates the coating thinning behaviour. The coating thickness is inversely proportional to the square root of the rotation speed: thickness~ $[1/\text{speed}]^{1/2}$ [22]. Apart from the edge effect an advantage of spin-coating is that film of liquid tends to become uniform in thickness during spin-off stage and, once uniform, tends to remain so provided that the viscosity is not shear dependant and does not vary over the substrate [22].

Flat and porous TiO_2 films by spin-coating

Several authors have reported on the deposition of flat TiO_2 films by sol-gel spin-coating technique using TTIP [39, 59- 62], TTET [31, 63, 64] or TTBU [63, 65] as Ti-source. The results mainly cover the film structural evolution upon annealing and the resulting morphology. However, in our study on flat TiO_2 films by spin-coating [31] as well as that by Vorotilov *et al.* [63], the electrical properties of TiO_2 films with the emphasis on their dielectrical properties have been reported. TiO_2-anatase films have yielded dielectric constant values of 23 [31] and 20-50 [63].
As we started our investigation into porous TiO_2 films deposition by sol-gel spin-coating technique in 2004, there were only articles published describing porous TiO_2 film deposition by sol-gel dip-coating (for example, see refs. 66, 67). Since that time (2005-2007) several publications have appeared on the formation of porous TiO_2 films by spin-coating technique, however.
In most cases polymers with a high molecular weight have been used as a pore directing agent [35, 68-70]. In this case the porosity of the obtained TiO_2 film is

controlled by the molecular weight or the amount of organic modifier in the precursor solution. Deposition of porous TiO_2 films without organic modifier has been published by Kim and Francis [71]. In their study the porous TiO_2 films have been deposited from the anhydrous TTET in EtOH solutions in atmospheres with high humidity (>20%). They have found that the use of higher titanium concentration in solutions and lower spinning rates resulted in coatings containing larger particles in more open microstructures [71]. Slooff *et al.* showed that the morphology of TiO_2 film is strongly dependent on the relative humidity during the coating with the TTIP-2-PrOH solution [72].

To summarize the ideas presented above, I would like to point out that flat TiO_2 films are mainly derived from solutions containing Ti-alkoxide together with stabiliser and solvent. In the case of spray pyrolysis many researchers have used "Tiacac" precursor for the film deposition. In order to obtain TiO_2 films with porous structure by spray pyrolysis (in literature also a term structured layer is often used [56]) mainly various solvents or substrate temperatures have been employed. However, for spin-coating deposition, the recent papers indicate formation of porous TiO_2 in the presence of structure directing agent in the sol-gel solution. To our knowledge, no complex studies on sol-gel spray pyrolysed flat TiO_2 films focusing on structure formation and electrical characterization have been performed.

1.5 TiO_2 as a window layer in solar cells

A revolutionary development in solar cell science and technology has been introduced in the form of electrochemical dye-sensitised solar cells by Grätzel and co-workers [11]. In this type of solar cell, nanostructured TiO_2 is made light sensitive with the help of only a monolayer of an organic dye.

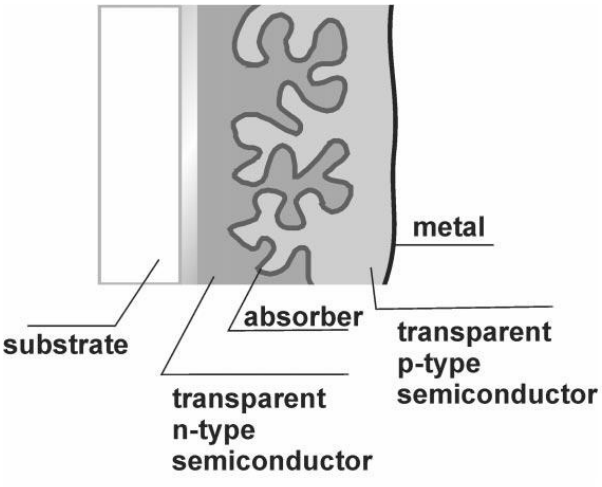

Figure 1.3. Schematic diagram of an eta-solar cell structure [12].

The so-called eta (extremely thin absorber)–solar cell is also based on this idea [12, 73]. In an eta-device (Fig. 1.3) only solid inorganic components are used and an extremely thin absorber (eta) is sandwiched between two wide-band gap semiconductors, one being n-type and the other p-type.

Table 1.2. Output characteristics of solar cells on flat and porous TiO_2 window layers

Structure of solar cell	**TiO_2**		**j_{SC}, mA/cm^2**	**V_{OC}, mV**	**FF, %**	**η, %**	**Ref.**
	F/P	Dep. method					
SnO_2:F/TiO_2/$In(OH)_xS_y$/ $CuInS_2$	F	CSP	10.7	450	44	2.1	[77]
SnO_2:F/TiO_2/Al_2O_3/ $In(OH)_xS_y$/$CuInS_2$	F	CSP	17.5	400	41	2.9	[81]
SnO_2:F/TiO_2/$In(OH)_xS_y$/ $CuInS_2$	F	CSP	14.6	456	43	2.9	[82]
SnO_2:F/TiO_2/$CuInS_2$/ CuSCN	P	CSP DB					[12]
SnO_2:F/TiO_2/CdTe	P	CSP	8.9	670	20		[76]
SnO_2:F/TiO_2/$Cd_xHg_{x-1}Te$	P	CSP	8.0	650			[75]
SnO_2:F/TiO_2/$In(OH)_xS_y$/ $CuInS_2$	P	DB	2.5	450	32	0.4	[77]
SnO_2:F/TiO_2/In_2S_3/ $CuInS_2$	P	DB	17.0	530	55	5	[78]
SnO_2:F/TiO_2/$In(OH)_xS_y$/ PbS/PEDOT:PSS	P	CSP	7.4	280	40	0.8	[80]
SnO_2:F/TiO_2/In_2S_3/ $CuInS_2$	P	DB				2.8	[79]

F-flat, P-porous, CSP-chemical spray pyrolysis, DB-doctor blading

The main advantage of this type of device is that the transport distance within the absorber is strongly reduced. As a consequence, the requirements for the electronic quality of the absorber material become less stringent and low-cost materials may be used in this type of device. In order to provide sufficient absorption of the light, highly structured *p–n* heterojunctions (nanoporous or microporous) must be used [74, 75]. In eta-solar cell structures, porous TiO_2 have been usually produced by doctor blading [12, 77- 79] or sol-gel spray pyrolysis [12, 75, 76]. Table 1.2 summarizes the reported results of solar cells based on flat or porous TiO_2 window layer with an inorganic absorber layer. As it can be seen, $In(OH)_xS_y$ is the favourable buffer layer whereas for the absorber layer a large variety of compounds have been used. So far, the best solar cell on spray deposited flat TiO_2 window layer in combination of wet chemically deposited indium sulfide buffer and $CuInS_2$ absorber layer has an efficiency of 2.9 %, and was prepared in our laboratory [80, 82]. The eta-solar cell on porous TiO_2 layer and sprayed $CuInS_2$ absorber layer has reached an efficiency as high as 5% [78]. From a theoretical point of view, solar

sells with extremely thin absorber layers may yield efficiencies larger than 10 % [83].

1.6 Summary of the literature review and the objective of the thesis

The studies on sol-gel precursors for TiO_2 films and sol-gel derived flat and porous TiO_2 films can be summarized as follows:

1. Prior reports have already mentioned the reaction that occurs between Ti-alkoxide and acetylacetone or 2-methoxyethanol as well as revealed the resulting plausible structure. The formation mechanism of sol-gel TiO_2 film by thermal analysis has only been studied for some precursor systems. No TA studies, to our knowledge, on the precursor system containing TTIP, acacH, and 2-MOE have been reported.
2. Flat sprayed TiO_2 films have been deposited from a large variety of precursors with emphasis on their structural, morphological and optical properties. However, electrical properties of sprayed flat TiO_2 films have been scarcely studied, some studies report of the conductivity measurements, however.
3. The formation of porous TiO_2 films by spray pyrolysis has been characterized for the effect of different solvents on the films microstructure. To our knowledge, prior to our studies, the development of porous TiO_2 films by spin-coating has been described as being the effect of humidity during the film deposition process. To our knowledge, no results on the formation of nanoporous TiO_2 films in the presence of structure directing agent (PEG) in solution using spray or spin coating techniques have been reported.
4. It has been recently demonstrated that the SnO_2:F/TiO_2/$In(OH)_xS_y$/PbS(O)/ PEDOT:PSS system deposited onto a sol-gel derived porous TiO_2 layer is suitable for photovoltaic applications. However, the specific role of $In(OH)_xS_y$ and PbS(O) layers and possible ways for optimization have not been demonstrated.

On the basis of the conclusions above, the objectives of the present doctoral thesis were:

1. To study the formation of TiO_2 films in sol-gel deposition process by comprehensive thermal analysis of dried TiO_2-gel powders, derived from the precursor system containing titanium(IV) tetraisopropoxide, acetylacetone and 2-methoxyethanol, by means of coupled techniques involving thermogravimetric and evolved gas analyses.
2. To study phase composition, morphology, optical and electrical properties of sprayed TiO_2 films depending on procedure variables, such as substrate and annealing temperature.

3. To deposit porous TiO_2 films by spray pyrolysis and spin-coating techniques using polyethylene glycol as a structure directing agent in the precursor solution. To characterize the morphology, composition and crystal structure of the TiO_2 films.
4. To study an complex eta-solar cell device (TiO_2/$In(OH_x)S_y$/PbS(O)/PEDOT:PSS) deposited onto a sol-gel derived porous TiO_2 layer by changing the deposition parameters such as the number of SILAR cycles and post-deposition annealing temperatures of $In(OH_x)S_y$ and PbS(O) layers as well as by incorporating a doped TiO_2 layer into the solar cell structure.

2 EXPERIMENTAL DETAILS

The main experimental features are briefly presented in this section. For details of the experiments, see publications I-VI.

2.1 Synthesis of the precursors by sol-gel method for thermoanalytical studies

The background of our studies is given in section 1.3. Briefly, based on the prior knowledge that TA studies of this precursor system (TTIP-acacH-2-MOE) have not been published and on the interest to find the proper temperature profile for TiO_2 film formation [32] we conducted TA studies (TG/DTA/DTG, coupled with EGA-FTIR and EGA-MS) to characterize our precursor system. In our studies [I, II] we have characterized sol-gel derived dried TiO_2 gel powders using the TTIP:acacH in molar ratios of 1 or 2 in the precursor solution.

2.1.1 Synthesis of xerogels

Synthesis of xerogels

Reagent grade chemicals, *viz.* titanium(IV) tetraisopropoxide (TTIP, $C_{12}H_{28}O_4Ti$, Merck), acetylacetone (acacH, $C_5H_8O_2$, Merck) and 2-methoxyethanol (2-MOE, $C_3H_8O_2$, Fluka) were employed for the synthesis as received, without any further purification.
Acetylacetone was added dropwise to TTIP in molar ratios of 1:1 and 2:1. The solutions were stirred for 30 mins at room temperature. The stabilized TTIP solutions were thereafter mixed with 2-MOE (TTIP:2-MOE=1:10) and refluxed at 130 ºC for 2 hours. The final solutions were cooled down to room temperature. To obtain the gel, the solution was allowed to slowly evaporate under ambient conditions. The dried gel powders, xerogels, used as samples for the thermal analysis, were labeled as Ti-1 (TTIP:acacH=1:1) [I, II] and Ti-2 (TTIP:acacH=1:2) [II].

2.1.2 Characterization of xerogels

Table 2.1 summarizes the analytical techniques used to characterize the xerogels. A more detailed explanation is given in [I] and [II].

Table 2.1. Analytical techniques used for the characterization of xerogels, TiO_2 films and eta-solar cells

	Properties	**Analytical technique**	**Apparatus**	**Ref.**
XEROGEL	composition	FTIR	Perkin Elmer GX1	[I, II]
	crystallinity, phase composition	XRD	Bruker AXS D5005 X'Pert Pro MPD	[I] [II]
	thermal decomposition temperatures	TG/DTG/DTA	Setaram Labsys 2000 STD 2960	[I] [II]
	evolved gases	TG/ EGA-FTIR TG/EGA-MS	Setaram Labsys 2000+ Ranger-AIR Gas cell S/N 23790 STD 2960+ Thermostar GSD 300	[I, II] [II]
	elemental composition	Elemental analysis of C, H	Gmbh Vario EL CHNOS Heraeus CHN-O-Rapid	[I] [II]
FILM	crystallinity and phase composition	XRD Raman FTIR	Bruker AXS D5005 Spex 340E monochromator Perkin Elmer GX-1	[III-V] [IV] [III-V]
	thickness	Ellipsometry SEM	DRE ELX-02C LEO SUPRA 35	[III,IV] [V]
	refractive index	Ellipsometry	DRE ELX-02C	[III,IV]
	morphology	SEM AFM	LEO SUPRA 35 SIS, Germany NT-MDT Smena+ MicroMasch CSC21	[V] [III] [IV]
	dielectric const., dielectric loss, thermal activation energy of conductivity	Impedance spectroscopy	Agilent 4192A	[III,IV] [IV] [IV]
eta-SC	SC output parameters	I-V	Keithley, SMU 237	[VI]
	SC quality	QE	Set-up (grating monochrom. + calibrated Si-photodiode + Keithley 428)	[VI]

2.2 Technological parameters for sol-gel derived TiO_2 films

2.2.1 Deposition of flat and porous TiO_2 films

Flat TiO_2 films were grown by sol-gel spray pyrolysis technique whereas porous TiO_2 films were deposited using sol-gel spin-coating and spray pyrolysis techniques. Technological scheme of TiO_2 films preparation is summarized in Table 2.2. More detailed explanation is presented in [III-V].

Table 2.2. Process parameters of TiO_2 film preparation

TiO_2	Film dep. tech.	Sol	Subst-rate	Deposition parameters	Annealing procedure	Ref.
FLAT	CSP	TTIP:acacH:EtOH 1:2:77 (molar ratio) [TTIP]= 6 vol.%	Si(100), HD Si(100)	Ts=300-500 ºC pulsed spray 1-3 cycles 1min spray+ 1min pause	500 ºC, 15 min; 700 ºC, 30 min; 800 ºC, 30 min in air	[III] [IV]
POROUS	CSP	TTIP:acacH:EtOH 1:2:52 (molar ratio) PEG600= 46g TTIP:PEG=1:7.7 (molar ratio) [TTIP]= 8.5 vol.%	Glass, Si(100)	Ts=350-500 ºC 30-50 cycles 10min spray+ 5min pause	500 ºC, 2h in air	[V]
	SC	TTIP:acac:EtOH 1:2:42 (molar ratio) PEG600= 1.5-46 g TTIP:PEG600= 1:0.25-7.7 (molar ratio) [TTIP]= 10.2 vol.%	Glass, Si(100)	RT 3 cycles at 3000 rpm	100 ºC, 35 min; 300-850 ºC, 1-2 h in air	[V]

CSP- chemical spray pyrolysis, SC – spin coating

2.2.2 Characterization of TiO_2 films

The analytical techniques used for the characterization of spin-coated and sprayed TiO_2 films are briefly summarized in Table 2.1. More detailed information about the instrumentation and measurements can be found in the experimental sections of [III-V].

2.3 Eta-type solar cell with TiO_2 window layer

Overview of the eta-type solar cell preparation and characterization is given in this section, more details can be found in [VI].

2.3.1 Preparation of eta-solar cell

Eta-solar cell structure, $TiO_2/In(OH)_xS_y/PbS(O)/PEDOT:PSS$, was deposited on glass substrates coated with SnO_2:F (TEC15, Pilkington). Firstly, sol-gel derived flat and porous TiO_2 layers, using TTIP as a Ti-source, were deposited by dip-coating method in the company Sglux (Berlin, Germany). For a given monolithic experiment, eight samples were cut out of one wafer having the size of 50x50 mm^2. By this way, samples with identical TiO_2 flat and porous layers were processed further by systematically changing one preparation parameter at a time. Secondly, $In(OH_x)S_y$ and PbS(O) layers were deposited by SILAR (Successive Ionic Layer Adsorption and Reaction) technique. The technological parameters changed during the $In(OH_x)S_y$ and PbS(O) layers deposition are summarized in Table 2.3. Finally, solar cells were completed by spin-coating of PEDOT:PSS (Baytron, Bayer Group, Leverkusen, Germany) as a hole conducting material followed by dropping colloidal graphite (G303, Plano GmbH, Wetzlar, Germany) onto the sample for the back contact. In some cases, the structured TiO_2 layer was modified by adding 2 at.% of $Nb(OC_2H_5)_5$ into the sol-gel solution.

Table 2.3. Optimization of $TiO_2/In(OH)_xS_y/PbS/PEDOT:PSS$ solar cell structure

Layer	Deposition	Annealing
$In(OH)_xS_y$	20-40 SILAR cycles, RT	Temp. region: RT-350 °C, Atmosphere: air
PbS	5-25 SILAR cycles, RT	Temp. region: RT-270 °C, Atmosphere: air

2.3.2 Characterization of eta-solar cell

The analytical techniques used to characterize the eta-solar cell structure, $TiO_2/In(OH_x)S_y/PbS(O)/PEDOT:PSS$ are summarized in Table 2.1. More detailed information about the instrumentation and measurements can be found in the experimental sections of [VI].

3 RESULTS AND DISCUSSION

3.1 TiO_2 formation in sol-gel deposition process

It was shown in my M.Sc. thesis [32] that TiO_2 films deposited by sol-gel spin-coating method, using TTIP stabilized with acacH in 2-MOE, yield materials with optical and dielectric properties similar to those obtained with titania, fabricated in more sophisticated and costly facilities. In order to gain a better understanding of the formation mechanism of TiO_2 films the thermal decomposition of dried gel powders was studied. We focused our attention on comparing thermal behaviour of dried titanium gels obtained by the gelling of acetylacetonate (acac)-modified titanium(IV) tetraisopropoxide (TTIP) in 2-methoxyethanol (2-MOE). Two gel powders were prepared based on Ti-alkoxide:acacH molar ratios of 1:1 (Ti-1) and 1:2 (Ti-2) and their thermal decomposition was monitored by simultaneous TG/DTA/DTG-FTIR and EGA-MS measurements [I, II].

3.1.1 Characterization of titanim(IV) acetylacetonate xerogels

The precursor gel powders (Ti-1 and Ti-2) for TiO_2 and the solid decomposition products of their thermal decomposition were characterized with the help of FTIR, elemental and XRD analyses. In this part a summary of the results is reported, more details can be found in [I, II].

FTIR study

FTIR spectra of the dried gel powders synthesised at the TTIP:acacH molar ratio of 1:1 (Ti-1) and 1:2 (Ti-2) are presented in Fig. 3.1. The assignment of absorption bands is presented in Table 3.1, based on the literature data [26, 33]. From a qualitative point of view, the FTIR spectra of the gel powders are similar and close to the spectra of $TiO(acac)_2$ (titanium(IV) oxide acetylacetonate; Aldrich-Sigma Product No. 3300833, Lot No 00408BE).
The formation of Ti(IV) acetylacetonate complexes is confirmed by two absorption bands centred at around 1580 and 1530 cm^{-1} which have been assigned to the ν(C-C) and ν(C-O) vibrations of acetylacetonato groups bound to titanium [33]. Unlike the Aldrich-Sigma product, $TiO(acac)_2$, Ti-1 and Ti-2 gel powders show an absorption at 1020 cm^{-1}. Sedlar and Sayer have recorded for the TTIP in methoxyethanol solution an absorption at 1022 cm^{-1} and assigned this to the C-O stretch of $Ti(OMOE)_4$ [26]. As FTIR spectra do not give any reliable proof of the presence of 2-MOE in the structure, we name the dried gel powders simply as titanium(IV) acetylacetonate. However, additional solid state MAS-NMR and pyrolysis GC-MS investigations might provide more information and knowledge needed to further characterize the precursor xerogels.

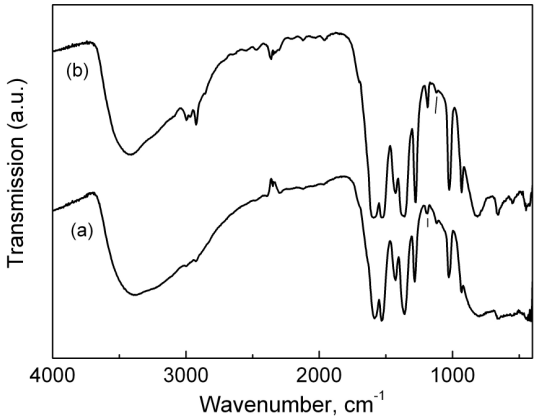

Figure 3.1. FTIR spectra of the dried gel powders: (a) Ti-1 (TTIP:acacH=1:1) and (b) Ti-2 (TTIP:acacH=1:2). The FTIR spectrum of Ti-1 is presented in [I].

Table 3.1. Assignment of vibrations in dried gel powders, Ti-1, Ti-2 and $TiO(acac)_2$ (Aldrich Sigma Product)

ν, cm^{-1}			**Assignment**	**Ref.**
Ti-1	**Ti-2**	**$TiO(acac)_2$**		
2999	2993	2994	(2980) ν(C-H):Pr^iOH, Pr^iO, acac	[33]
1583	1588	1600	(1590) ν(C-C) + ν(C-O):acac	[33]
1531	1526	1525	(1530) ν(C-C) + ν(C-O):acac	[33]
1427	1426	1424	(1430) $\delta(CH_3)$:Pr^iOH, Pr^iO, acac	[33]
	~1380	1383	(1380) $\delta(CH_3)$:Pr^iOH, Pr^iO, acac	[33]
1360	1360	1356	(1330) ν(C-CH_3):Pr^iOH, Pr^iO (1370) δ_s(C-H):OMOE	[33] [26]
1283	1276	1273	(1280) ν(C-CH_3):acac	[33]
1185	1185	1181	(1165) $\gamma_s(CH_3)$:Pr^iOH, Pr^iO (1170) γ(C-H): Pr^iO	[33] [26]
1120	1120	-	(1125) ν(C-O-C):OMOE, HOMOE	[26]
1028	1025	1024	(1015) ν(C-O):Pr^iO	[33]
932	931	932	(930) ν(C-O):Pr^iOH + n(C-CH_3)acac	[33]
792	812	822	(820) $\gamma_a(CH_3)$:Pr^iOH	[33]
661	661	661	(665) γ(CH_3-CO-C):acac	[33]
435	430	438	(440) ν(Ti-O):acac	[33]

According to the elemental analysis, carbon content in precursor xerogels was found to be 18.91 and 27.76 mass% and that of hydrogen 3.24 and 3.35 mass% for Ti-1 and Ti-2, respectively.

XRD profiles show that the precursor xerogels are amorphous, but Ti-1 shows a broad peak centred at ca. 2Θ= 6°, which could be interpreted as indicating a ca. *d*=15 Å average pore-size with a certain pore-size distribution [84].

3.1.2 Thermal analysis of titanium(IV) acetylacetonate xerogels

The thermal decomposition process of titanium(IV) acetylacetonate xerogels serving a precursors for TiO_2 films was characterized with the help of TG/DTG/DTA in air using the heating rates of 5 ºC min^{-1} (Ti-1, TTIP:acacH=1:1) [I] or 10 ºC min^{-1} (Ti-1, TTIP:acacH=1:1; Ti-2, TTIP:acacH=1:2) [II]. For clarity of the obtained results, the results on TA are first discussed for the samples monitored with the heating rate of 10 ºC min^{-1}. Followed by the results obtained for the solid decomposition products of the Ti-1 sample recorded with the heating rate of 5 ºC min^{-1}.
According to the DTG curve, six mass loss steps could be detected for Ti-1 (Fig. 3.2) and Ti-2 (Fig. 3.3) when the heating rate of 10 ºC min^{-1} was used.

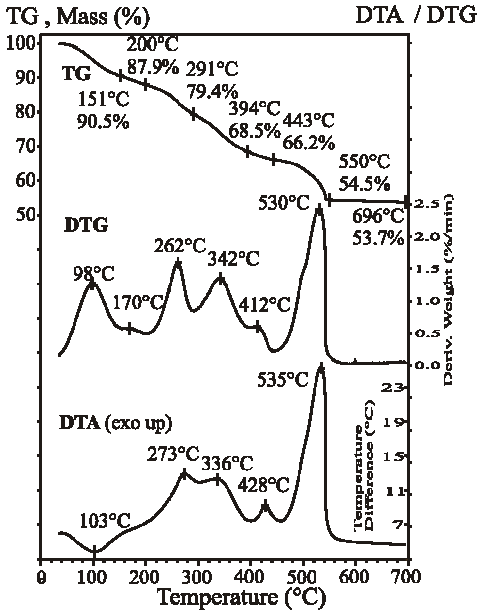

Figure 3.2. Simultaneous TG, DTG and DTA curves of Ti-1 (TTIP:acacH=1:1) recorded in flowing air of 130 mL min^{-1} using the heating rate of 10 °C min^{-1}. The sample mass is 38.82 mg.

For Ti-1 (Fig. 3.2) the first mass loss step between 30-151 ºC in an endothermic reaction with a mass loss of 9.5 %. The following DTG maxima (2, 3, 4, 5, 6) at 170, 262, 342, 412, 530 ºC, respectively, are exothermic reactions according to DTA. The step 2, however, is very small as the observed weight loss is below 3 %. In contrast, for Ti-2 with its higher acac content, the second step is a significant one as seen in all TA curves (*cf.* Figs. 3.2, 3.5, 3.7). According to the TG curve, the total mass loss in the temperature interval of 30-700 ºC is 46.3 %. When the heating rate of 5 ºC min^{-1} was used, five mass loss steps could be detected for Ti-1 and the total mass loss in the temperature interval of 30-900 ºC was slightly less or

43.8 % [I]. As expected, the lower heating rate (5 *vs.* 10 ºC min^{-1}) moves the starting of decomposition towards lower temperatures by some tens of degrees.
For Ti-2 (Fig. 3.3) the first mass loss step between 30-122 ºC is an endothermic reaction with a mass loss of 4.1 %. The following DTG maxima (2, 3, 4, 5, 6) at 191, 264, 319, 457 and 507 ºC, respectively, are exothermic reactions according to DTA. The TG curve shows then an insignificant weight drop at temperatures above 500 ºC. The total mass loss in the temperature region of 30-700 ºC is 54.4 %. The increased content of organic matter (acac) in the case of Ti-2 is visible as an additional, strong DTG peak at 191 ºC as well as in the EGA patterns where the maximum acacH evolution at 195 ºC coincides with this temperature.

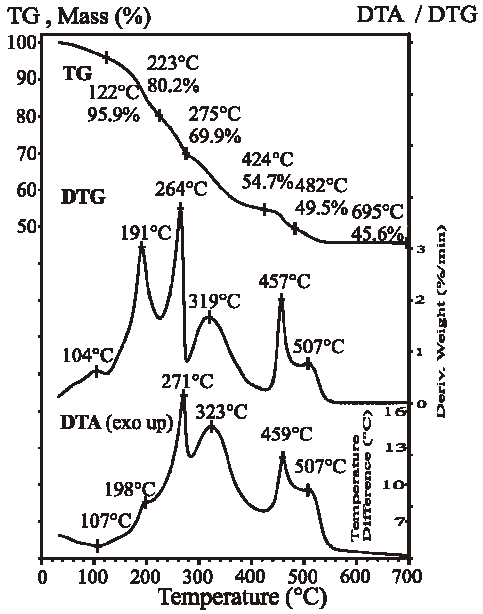

Figure 3.3. Simultaneous TG, DTG and DTA curves of Ti-2 (TTIP:acacH=1:2) recorded in flowing air of 130 mL min^{-1} using the heating rate of 10 °C min^{-1}. The sample mass is 33.52 mg.

The first decomposition step for both Ti-1 and Ti-2 consists of the evolution of water as confirmed by both MS (*cf.* chapter on Evolved gas analysis) and EGA-FTIR [I]. Main difference in the decomposition behaviour of the xerogels studied, Ti-1 and Ti-2, is observed in the first three decomposition steps (30-291 ºC for Ti-1 and 30-275 ºC for Ti-2), showing quite different total mass losses of 20.6 % and 30.1 %, respectively. The mass losses in the following decomposition steps 4-6 (in the temperature region from about 300 ºC up to 700 ºC) resemble each other (Figs. 3.2, 3.3), giving 25.7 % for Ti-1 and 24.3 % for Ti-2. The decompositions of Ti-1 and Ti-2 are completed at almost same temperatures, *viz.* 550 ºC and 540 ºC, respectively.

Final decomposition products of Ti-1 and Ti-2 were determined by XRD, while the intermediates of Ti-1 decomposition obtained using the heating rate of 5 ºC min^{-1} were characterized with the help of FTIR, XRD and carbon content measurements [I]. FTIR spectra of the solid decomposition products of the Ti-1 sample heated up to 150, 275, 410 and 510 °C are presented in Fig.3.4. According to FTIR, the only difference in the sample heated up to 150 ºC, as compared to the precursor (Fig. 3.1a), is the weakening in intensity of a broad absorption band in the region of 3600-3200 cm^{-1}, characteristic to water and hydroxyl groups. The product at 275 ºC shows a significantly different FTIR spectrum, however. The absorptions around 3400 cm^{-1} are weakened in intensity, and the vibrations at 1360, 1280, 1200-1100 and 930 cm^{-1}, are vanished (Table 3.1). The vibrations at 1590-1530 cm^{-1} and the absorption at 1706 cm^{-1}, characteristic to C=O bonding [26], are still present in the sample, however. The decomposition product at 410 °C shows only very weak absorptions at 1520 and 1370 cm^{-1}. IR spectrum of the sample prepared at 510 °C shows a broad absorption in the region of 1000-400 cm^{-1}, characteristic to a Ti-O-Ti network [46].

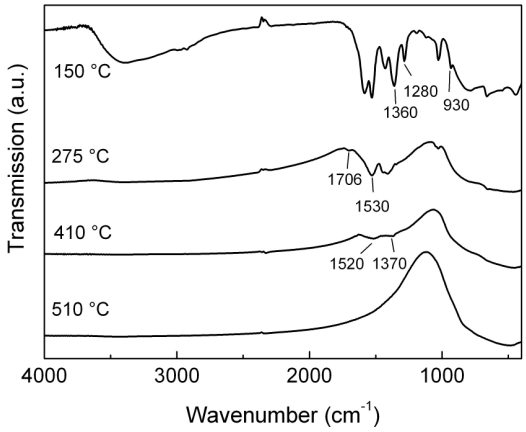

Figure 3.4. FTIR spectra of solid intermediates of the Ti-1 sample prepared at 150, 275, 410 and 510 °C with the heating rate of 5 °C min^{-1}.

XRD studies reveal that crystalline anatase phase is the decomposition product around 500 °C while crystalline rutile appears above 800 ºC. The solid intermediates at lower temperatures are all amorphous. According to the elemental analysis, the carbon content increases when going from room temperature up to 150 ºC. Further annealing decreases the carbon content from 21.8 to 10.1 mass% with increasing the temperature from 150 to 410 ºC and around 500 ºC carbon is present in trace amounts only (< 0.1 mass%).

A calculation based on RIR (reference intensity ratio) data of the reference patterns [85] indicates that the solid residues obtained at 700 °C in air with the heating rate of 10 ºC min^{-1} contain rutile (JCPDS-PDF 21-1272) and anatase (JCPDS-PDF 21-1276) in an approximate ratio of 72:28 and 26:74 for Ti-1 and Ti-2, respectively.

The anatase-rutile transformation temperature (800 ºC) is the same as found by Suresh et al. using acetic acid modified gel precursor [86]. However, depending on the ligands and additives on the system, the transformation temperature may be significantly different [87, 88].

3.1.3 Evolved gas analysis of titanium(IV) acetylacetonate xerogels by FTIR

Our first attempt [I] on the characterization of evolved gases by EGA-FTIR showed that the first mass loss step of Ti-1 (30-151 ºC) corresponds to the evolution of H_2O. To avoid the overlapping of the IR vibrations of evolved gases and water at higher temperatures, the precursors were pre-heated up to 120 ºC. Pre-heated Ti-1 and Ti-2 were then used as a precursors for the simultaneous TG/DTA coupled with EGA-FTIR analysis using the heating rates of 5 ºC min^{-1} (Ti-1, TTIP:acacH=1:1) [I] or 10 ºC min^{-1} (Ti-1, TTIP:acacH=1:1; Ti-2, TTIP:acacH=1:2) [II]. In this section the results on the evolved gas analysis are discussed in more detail for the xerogels measured with the heating rate of 10 ºC min^{-1} [II]. The results of Ti-1 sample are compared with the obtained results when heating rate of 5 ºC min^{-1} [I] was used. In order to identify the evolved gases, the measured spectra were analysed by taking the reference spectra from the database (NIST) and comparing them to the evolved gas spectra at different temperatures.

Figures 3.5 and 3.6 show the derivative gas evolution profiles (Ti-1 and Ti-2, respectively), obtained as derivatives of the peak intensities (dI/dt) or the peak areas (dS/dt), and integrated above the FTIR spectrum baseline. The temperatures for gas evolution and temperatures of the evolution maxima ($dI/dt=0$) are marked in the figures. For CO_2, the peak areas in the region of 2215-2405 cm^{-1} were used for the calculations. The non-overlapping C=O vibrations were used to identify the evolved gases: acetic acid (CH_3COOH, 1773 cm^{-1}), acetone (CH_3COCH_3, 1746 cm^{-1}), and acetylacetone ($CH_3COCH_2COCH_3$, 1623 cm^{-1}). Using this procedure, all absorptions of the measured spectra could be matched with the gas spectra from the database, except for the absorption band recorded in the region 1027-1100 cm^{-1} (with the maximum at 1060 cm^{-1}) which does not match with any of the above-mentioned gas spectra.

In the case of Ti-1 (Fig. 3.5), the main evolved gases in the temperature interval of 100-310 ºC are acetone and acetic acid which most probably are the decomposition products of acetylacetone [89]. The intensities of the characteristic peaks of acetone and acetic acid reach their maxima at 290-310 ºC, being typical for the decomposition step 3. Evolution of CO_2 starts at 160 ºC and its evolution maxima are located at 365, 390, 435 and 540 ºC.

In the case of Ti-2 (Fig.3.6), the initially evolved gas is acetylacetone reaching its maximum at 210 ºC and being characteristic for the decomposition step 2. Acetone and acetic acid with their evolution maxima at 280 ºC and 300 ºC, respectively, are showing only about half of the evaporation intensity of acetylacetone. Evolution of CO_2 starts at 155 ºC and it is continuously evolving also during the next decomposition steps showing maxima at 375, 415 and 500 ºC.

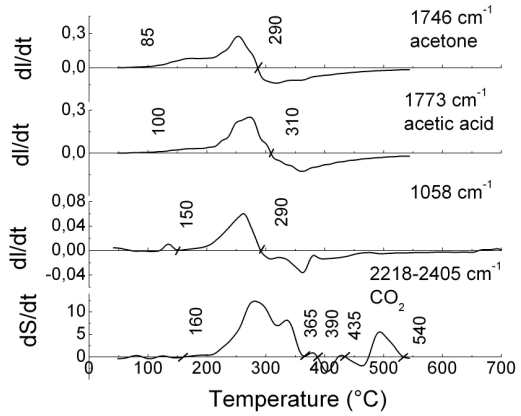

Figure 3.5. Derivative evolution profiles of gases as determined by EGA-FTIR for Ti-1 (1:1). The curves are recorded in flowing air of 130 mL min^{-1} using the heating rate of 10 °C min^{-1}. The sample mass is 33.4 mg. The sample was pre-heated in air up to 120 °C. The starting and maximum temperatures (dI/dt=0) of gas evolution are also given.

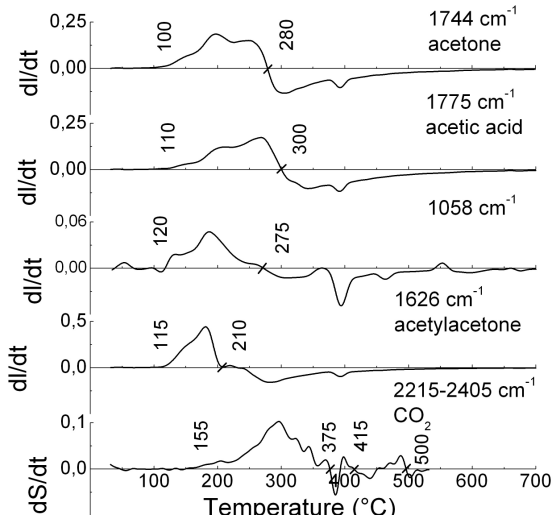

Figure 3.6. Derivative evolution profiles of gases as determined by EGA-FTIR for Ti-2 (1:2). The curves are recorded in flowing air of 130 mL min^{-1} using the heating rate of 10 °C min^{-1}. The sample mass is 37.3 mg. The sample was pre-heated in air up to 120 °C. The starting and maximum temperatures (dI/dt=0) of gas evolution are also given.

Unfortunately, EGA-FTIR does not unambiguously distinguish evolved gases due to the overlapping of their characteristic vibrations. Therefore, the evolved gases were characterized also by MS analyses.

3.1.4 Evolved gas analysis of titanium(IV) acetylacetonate xerogels by MS

The results on simultaneous TG/DTA/EGA-MS measurements of Ti-1 and Ti-2 samples, monitored with the heating rate of 10 ºC min^{-1}, are reported in [II].
Figures 3.7 and 3.8 show the evolution profiles of evolved gaseous species from the xerogels Ti-1 and Ti-2, respectively. The decomposition starts with the evolution of H_2O, having a well-shaped maximum at 115 ºC irrespective of the sample. Hence, the endothermic peaks at 98 and 104 ºC in the DTG curves (Fig. 3.2 and 3.3) of Ti-1 and Ti-2, respectively, can be assigned as belonging to H_2O. According to the TG-MS analysis, the main evolution of organic molecular species occurs at temperatures above 100 ºC and is characteristic for the decomposition steps 2 and 3 in the TG curves (Fig. 3.2 and 3.3). Partial oxidation of the organic constituents also takes place in each decomposition step from 3 to 6, which is indicated by their exothermic heat effects and by the more or less continuous formation of H_2O (*m/z*= 18) and CO_2 (*m/z*= 44) as the oxidation products in these steps (Fig. 3.7 and 3.8).
In the case of Ti-1, evolution of acetone (*m/z*=58, CH_3COCH_3) starts around 115 ºC and reaches a constant level between 195 and 220 ºC. The evolution continues in the third decomposition step with its maximum at 260 ºC. The evolution of acetic acid (*m/z*= 60, CH_3COOH), observed in the temperature range of 150-350 ºC, is characteristic for the third decomposition step. Evolution of acetone and acetic acid was also detected by the EGA-FTIR measurements as discussed above. In addition, gaseous species with *m/z*= 72, 74, 75, showing similar evolution profiles, were observed (presented by *m/z*= 74 in Fig. 3.7). It could be speculated that the methoxyethoxy group is present in the structure of the precursor as reported for the Zn-alkoxides in 2-MOE [90, 91]. The gaseous species with intense ion fragment of *m/z*= 74 could belong to 2-methoxy-acetaldehyde (Figs. 3.7 and 3.8). Nevertheless, the presence of several other $C_3H_6O_2$ compounds with the molecular ion fragment of *m/z*=74, such as propanoic acid, ethyl formate, methyl acetate or 3-hydroxypropane aldehyde, can not be excluded.
In the case of Ti-2, the main gaseous species released in the second step is acetylacetone (main characteristic fragments *m/z*= 85 and 100, *viz.* $CH_3COCH_2COCH_3$) with the maximum at 195 °C (presented by *m/z*= 85 in Fig. 3.8). Simultaneously, a partial evolution of acetone and acetic acid appears to begin, indicated by the appearance of ion fragments *m/z*= 58 and *m/z*= 60, respectively. The maximum evolution of acetone and acetic acid was observed in step 3, together with that of *m/z*= 74 which occurred at 265 ºC (Fig. 3.8). Similar products, *viz.* acetylacetone, acetone, acetic acid, CO_2 and CO were observed by high resolution MS during the thermal decomposition of Cu(II)-acetylacetonate [89]. Altogether, the intense evolution of acetylacetone from the sample Ti-2 (TTIP:acacH=1:2) in the decomposition step 2 is the main difference compared to Ti-1 (TTIP:acacH=1:1), where no release of acetylacetone was observed.

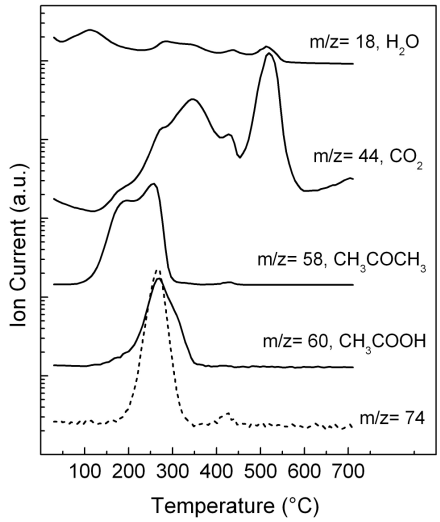

Figure 3.7. Evolution profiles of gaseous species as monitored by TG/DTA-EGA-MS for the sample Ti-1 (1:1). The curves are recorded in flowing air of 130 mL min^{-1} using the heating rate of 10 ºC min^{-1}; the sample mass is 38.82 mg.

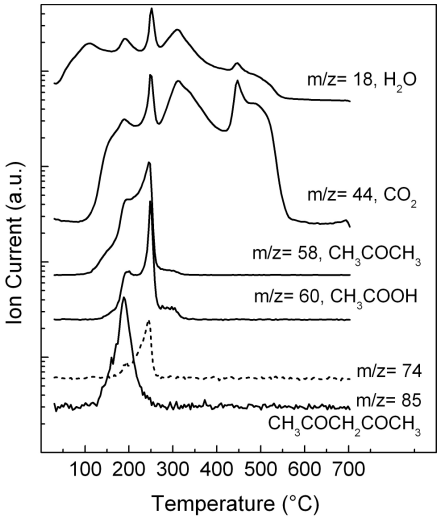

Figure 3.8. Evolution profiles of gaseous species as monitored by TG/DTA-EGA -MS for the Ti-2 (1:2). The curves are recorded in flowing air of 130 mL min^{-1} using the heating rate of 10 ºC min^{-1}; the sample mass is 33.52 mg

We did not observe the evolution of either alcohols (2-PrOH, or 2-MOE) or propene ($CH_3CH=CH_2$) either by MS or EGA-FTIR. However, Campostrini *et al.* have recently reported the evolution of 2-PrOH and propene from the Ti(IV) isopropoxide complexes with formic, acetic or oxalic acids at temperatures up to 300 ºC using combined TG-GC-MS [28, 40-42]. In case of gels modified by oxalic acid, the isopropanol and propene evolve already at 125 °C [40]. This may indicate that the boiling step at 130 °C used in our experiment to prepare the sol could be effective enough to completely eliminate the isopropoxide moieties.

A summary of the results on simultaneous TG/DTA/EGA-FTIR and -MS measurements is presented in Table 3.2. Thermal degradation of the Ti-1 and Ti-2 xerogels in the temperature range of 30-700 ºC consists of 6 mass loss steps with the total mass loss of 46.3 % and 54.4 %, respectively. The samples studied release only water up to 120 ºC. The further decomposition steps are exothermic and include the evolution of CO_2 and H_2O, arising from burning of the organic residues up to 550 °C. In the temperature region of 120-320 ºC, the main released gases were acetone and acetic acid released from both precursors, as well as acetylacetone evolved from Ti-2 only, as shown by both EGA-FTIR and EGA-MS. In addition, according to EGA-MS, the gaseous species with m/z= 74 was evolved from both xerogels at temperatures above 200 °C.

Table 3.2. Summary of the results on simultaneous TG/DTA/EGA-FTIR and -MS measurements of dried gel powders of Ti-1 and Ti-2 recorded using the heating rate of 10 ºC min^{-1}

Step	**Ti-1**					**Ti-2**				
	Temp range, ºC	+/-	Δm, %	Gases	Product	Temp range, ºC	+/-	Δm, %	Gases	Product
1	30-151	endo	9.5	H_2O	amorph.	30-122	endo	4.1	H_2O	amorph.
2	151-200	exo	2.6	CH_3COCH_3 CH_3COOH H_2O, CO_2	-	122-223	exo	15.7	$CH_3COCH_2COCH_3$ CH_3COCH_3 CH_3COOH H_2O, CO_2	-
3	200-291	exo	8.5	CH_3COCH_3 CH_3COOH m/z=74 H_2O, CO_2	-	223-275	exo	10.3	CH_3COCH_3 CH_3COOH m/z=74 H_2O, CO_2	-
4	291-394	exo	10.9	H_2O, CO_2	-	275-424	exo	15.2	H_2O, CO_2	-
5	394-443	exo	2.3	H_2O, CO_2	-	424-482	exo	5.2	H_2O, CO_2	-
6	443-700	exo	12.5	H_2O, CO_2	R:A= 72:28	482-700	exo	3.9	H_2O, CO_2	R:A= 26:74

A- anatase, R- rutile

3.2 Flat TiO_2 films by sol-gel method

The spray pyrolysed TiO_2 films by the sol-gel method were deposited from a solution containing TTIP as Ti-source, acacH as stabilizer and EtOH as solvent with TTIP concentration of 6 vol.% and TTIP:acacH molar ratio of 1:2 (see Table 2.2 in section 2.2.1). The films were deposited onto silicon wafers at substrate temperatures (T_S) between 315 and 500 °C using pulsed spray solution feed. The final annealing (T_{AN}) of the TiO_2 films was performed at 500, 700 [III, IV] or 800 °C [IV] in air. The structural (FTIR, XRD, Raman), optical (UV-VIS, ellipsometry), morphological (AFM) and electrical (Impedance spectroscopy) properties of sprayed TiO_2 films are presented in [III, IV].

3.2.1 Structural study of flat TiO_2 films

FTIR study

IR-spectroscopy has been used to study the effect of deposition and annealing temperatures on the formation of TiO_2 films deposited by spray pyrolysis [III].
The as-deposited TiO_2 films sprayed at T_S= 315-435 °C (Fig. 3.9) show absorptions at 1545, 1452 and 1415 cm^{-1} which could belong to asymmetrical and symmetrical vibrations of M-O-C and CH_2 or CH_3 groups, respectively [92-94].

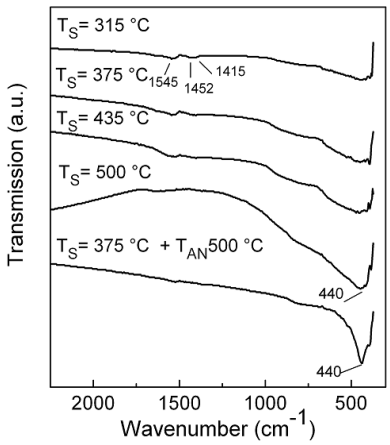

Figure 3.9. FTIR spectra of sprayed TiO_2 films deposited at different substrate temperatures (T_S) and a spectrum of the TiO_2 film deposited at Ts=375 °C and annealed at T_{AN}=500 °C.

The absence of above-mentioned absorptions at T_S= 500 °C shows that TiO_2 films free of organic residues could be grown at this temperature. Post-deposition annealing at 500 °C results in a well defined absorption peak at 436 cm^{-1}, independent of the deposition temperature. This corresponds to the formation Ti─O─Ti network and the development of a TiO_2-anatase structure [46]. TiO_2

films deposited below 400 °C remain anatase after annealing at 700 °C (Fig. 3.10) whereas the films grown at 435 °C show the absorptions of the anatase phase and an additional absorption peak at 496 cm^{-1}, which can be attributed to the rutile phase. IR-spectrum of TiO_2 film deposited at 500 °C and annealed at 700 °C clearly shows the absorptions at 420, 498 and 678 cm^{-1} characteristic for the rutile phase [46]. In addition, an absorption band close to 1060 cm^{-1} appears (Fig. 3.10, T_S=500 ºC) which can be attributed to the stretching mode of Si-O bond [46] suggesting SiO_2 formation at the interface during the annealing.

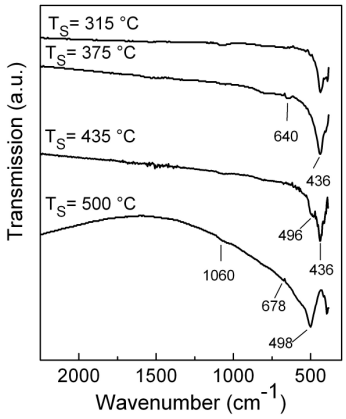

Figure 3.10. FTIR spectra of the sprayed TiO_2 films deposited at different substrate temperatures (T_S) and annealed at 700 °C for 30 min in static air.

It should be mentioned that annealing at 800 °C did not lead to any structural changes of the TiO_2 films as compared to those annealed at 700 °C.

XRD study

XRD study was applied to characterize the crystal structure evolution and degree of crystallinity in the sprayed TiO_2 films. The results are published in [III].
According to XRD, TiO_2 films sprayed at substrate temperatures below 500 °C are amorphous. The (101) peak of anatase (JCPDS-PDF 21-1272) becomes apparent for the films deposited at 500 °C (Fig. 3.11). Annealing at 500 °C results in films with crystalline anatase phase regardless of the deposition temperature. TiO_2 films deposited below 400 °C and subjected to annealing at 700 °C remain anatase whereas the films grown at 435 °C are composed of anatase and rutile (JCPDS-PDF 21-1276) phases. TiO_2 films grown at 500 °C and annealed at 700 °C result in pure rutile state. Annealing at 800 °C promotes the formation of TiO_2-rutile provided that the films are deposited above 400 °C; however, the films deposited below 400 °C remain anatase.
According to the literature crystalline TiO_2-anatase films by spray pyrolysis were obtained at deposition temperatures between 400 and 450 °C from solutions

containing commercial non-specified "Tiacac" [38, 46] or TTIP in alcohol solutions [47, 50]. Using TTIP and acacH in a molar ratio of 1:1 in the precursor solution leads to crystalline TiO_2-anatase films between 400 and 500 °C [54].

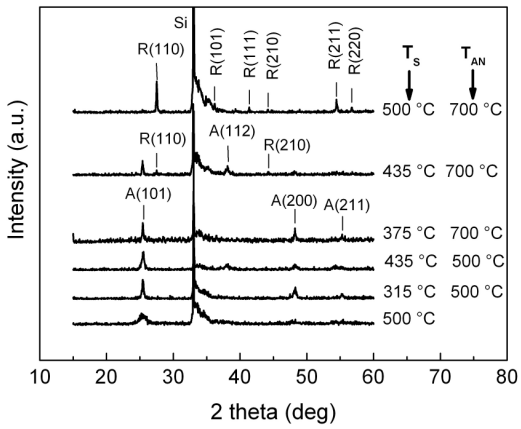

Figure 3.11. XRD patterns of as-deposited and annealed TiO_2 films.

The change in the crystalline structure (from anatase to rutile) after annealing at temperatures of the order of 800 °C is in agreement with several reports [46, 47].
The mean crystallite size was calculated from the (101) peak of anatase or the (110) peak of rutile phase on the XRD patterns using the Scherrer formula. For sprayed TiO_2 films the mean crystallite size is found to increase with the annealing temperature (from 700 to 800 °C) from 30 nm to 59 nm for the TiO_2-anatase films (T_S< 400 °C) and from 50 nm to 86 nm for the TiO_2-rutile films (T_S> 400 °C). The estimated grain size values are comparable with the values presented in the literature for the spray deposited TiO_2 films where the values of 20-26 nm [50] and 49-56 nm [54] for anatase structure and 31 nm [50] and 77-128 nm [38] for rutile have been reported. For example, grain size values for TiO_2-anatase films have been found to be 28 nm by sol-gel spin coating [31].

Raman study

Raman spectroscopy measurements were carried out to detect and identify the crystallization of the TiO_2 layer. Results on the Raman spectroscopy studies of sprayed TiO_2 films are published in [IV].
Raman spectra of TiO_2 films deposited at $T_S \leq$ 435 °C and annealed at 700 °C (Fig. 3.12) reveal anatase phase as peaks at 148, 200, 399 and 641 cm^{-1}, belonging to the E_g, E_g, B_{1g}, E_g, anatase modes, are present [95]. The films grown at 500 °C and annealed at 700 °C clearly show the peaks at 442 and 617 cm^{-1}, characteristic of the TiO_2-rutile absorption modes [96].

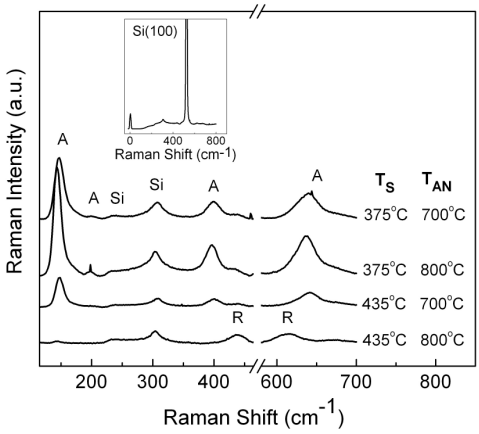

Figure 3.12. Raman spectra of TiO_2 films deposited at different temperatures (T_S) and annealed (T_{AN}) at 700 and 800 °C.

Upon annealing at 800 °C, the sprayed TiO_2 films deposited below 400 °C and above 400 °C remain anatase and rutile, respectively (Fig. 3.12). The spectra associated with the films deposited below 400 °C indicate the narrowing of the bands and the shift in the peak positions (Fig. 3.12). After the heat-treatment at 800 °C the main anatase peak at 148 cm^{-1}, characteristic for the films annealed at 700 °C, shifts to 144 cm^{-1}. Similar shift was observed for the TiO_2 nanophase samples annealed in air [97] as well as for the spray and CVD deposited TiO_2 films [98]. The shift in the Raman peak position has been assigned to non-stoichiometry of the samples [97, 98].
The full width at half maximum (FWHM) of the main anatase peak of the films grown below 400 °C decreases from 17±0.7 to 14±0.7 cm^{-1} when increasing the annealing temperature from 700 to 800 °C, indicating a structural improvement.

Summary of the structural study of flat TiO_2 films

FTIR, XRD and Raman results indicate that TiO_2 films deposited by spray pyrolysis of acacH-stabilized TTIP solutions in EtOH at substrate temperatures below 400 °C remain anatase even after annealing at 800 °C (Table 3.3).

Table 3.3. Summary of structural studies of sprayed TiO_2 films by FTIR, Raman and XRD. T_S- substrate temperature, T_{AN}- annealing temperature

	T_S, ˚C	T_{AN}= 500 ˚C		T_{AN}= 700 ˚C			T_{AN}= 800 ˚C		
		FTIR	XRD	FTIR	Raman	XRD	FTIR	Raman	XRD
Spray pyrolysis	375	A	-	A	A	A	A	A	A
	435	A	-	A+R	A	A+R	R+A	R	R
	500	A	A	R	R	R	R	R	R

A- anatase, R- rutile

According to XRD, the sprayed TiO_2 films grown at 435 °C and annealed at 700 °C show crystalline anatase structure, which turns to crystalline rutile by annealing at 800 °C. However, at both annealing temperatures a mixture of anatase and rutile phases were present according to the IR spectra. Spray deposition at 500 °C followed by annealing at 700 °C or at higher temperatures result in TiO_2 rutile phase as confirmed by FTIR, XRD and Raman measurements.
Thus it can be concluded that the structure of the sprayed TiO_2 films can easily be modified by the substrate or annealing temperatures.

3.2.2 Optical properties and morphology of flat TiO_2 films

Ellipsometric study

Ellipsometric study was conducted in order to determine thickness and refractive index of the sprayed TiO_2 films. The results are published in [III, IV].
Sprayed TiO_2 films deposited at substrate temperatures of 315, 375, 435 and 500 °C using a single spray pulse and subsequently annealed at 700 °C show thicknesses of 60, 90, 100 and 120 nm, respectively. The refractive index of sprayed TiO_2-anatase films increases from 2.1 up to 2.3 if the annealing temperature rises from 700 °C up to 800 °C indicating film densification. A lowering in the film thickness together with the increase in the film refractive index (from 2.2 up to 2.6) has been observed if the annealing temperature for the film deposited at 435 °C is increased from 700 °C to 800 °C. Such behaviour is in agreement with the structural changes (see section. 3.2.1, XRD study).
In addition, the annealing above 700 °C promotes the growth of an interfacial SiO_2 layer at the Si/TiO_2 interface, confirmed also by an absorption around 1060 cm^{-1} in the FTIR spectra (see section 3.2.1, FTIR study). According to the ellipsometric measurements, the thickness of SiO_2 layer increases from an average of 5 nm to 10-20 nm by annealing at 700 °C and 800 °C, respectively. The presence of the SiO_2 layer is taken into account in the electrical characterization of the films (see section 3.2.3).
The refractive index values are in agreement with the literature values reported for the TiO_2-anatase thin films, *viz.* 2.2 by spin coating [31], 1.8-2.3 by spray pyrolysis [46], and 2.4 by ALD [99] as well as by LP-MOCVD [100]. For sprayed and annealed TiO_2-rutile films refractive index of 2.7 has been reported [46].

AFM study

AFM studies have been performed in order to characterize the surface roughness of the sprayed TiO_2 films and the results are presented in [III, IV].
Our studies showed that the surface roughness of the spray pyrolysed TiO_2 films deposited below 500 °C approximately doubles with the increase of the annealing temperature from 700 °C to 800 °C.

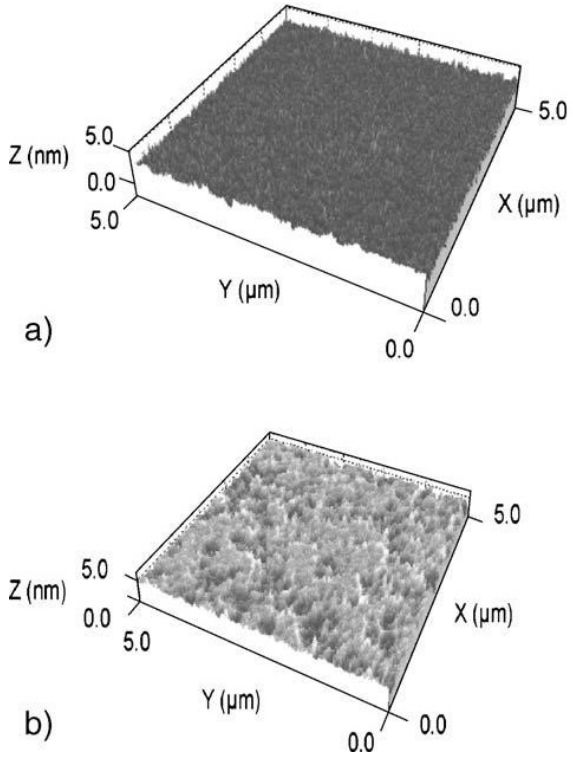

Figure 3.13. AFM images of TiO_2 films deposited by spraying at 435 °C and annealed at (a) 700 and (b) 800 °C.

The rms roughness of the TiO_2 films deposited at 375 °C is 0.6 nm and 1.1 nm after the annealing at 700 and 800 °C, respectively. For the films deposited at 435 °C the rms roughness was determined to be 0.35 nm and 0.70 nm after annealing at 700 and 800 °C, respectively (Fig. 3.13). The increase of the surface roughness with annealing temperature is caused by increased crystallite size as shown by XRD studies. However, the increase of the annealing temperature has much weaker effect on the roughness of the samples deposited at 500 °C.
According to the literature, TiO_2 anatase films grown by spray pyrolysis exhibit rms roughness values of 0.5-22.5 [47], 4.2-11.4 [46]. Our previous studies on spin-coated TiO_2-anatase films indicated rms roughness of 1.7 nm [31].

3.2.3 Electrical properties of flat sprayed TiO_2 films

We initiated the electrical characterization of sol-gel derived spray pyrolysis deposited flat TiO_2 films during the WTZ project with emphasis on the dielectric properties of TiO_2 films. Electrical properties of sprayed TiO_2 films are acquired from impedance measurements and results are presented in [III] and [IV].

Effective dielectric constant of sprayed TiO_2 films

Impedance spectroscopy measurements were carried out on the thermally annealed TiO_2 films on silicon substrates. In this kind of system, an interfacial SiO_2 layer forms during annealing, resulting in the following structure: $Si/SiO_2/TiO_2$. The formation of interfacial SiO_2 layer was confirmed by FTIR and ellipsometric measurements (see sections 3.2.1 and 3.2.2). The capacitance *vs.* frequency (C *vs.* F) measurements were carried out in order to determine the effective dielectric constant (ε) values for the sprayed TiO_2 films. In our studies [31,32, III, IV], ε was calculated from the slope of the linear fit of the reciprocal of capacitance (1/C) at 10 kHz *vs.* film thickness. The calculation is reported in detail in [31, 32]. Effective dielectric constant value for the sprayed films depends on the deposition temperature. For the sprayed TiO_2-anatase and -rutile films the calculated ε values, regardless of the annealing temperature, were between 36- 46 (±5) and 53- 70 (±5), respectively.
In contrast, effective dielectric constant of spin-coated TiO_2-anatase film was found to be 23±5 if the same precursor solution was used [32]. In comparison the dielectric constant values reported in the literature for the TiO_2 films deposited by vapour- phase deposition methods (ALD, CVD, sputtering, MOCVD) vary in the range of 19-76 for TiO_2-anatase [101-106] and 58-100 for TiO_2-rutile [101, 102, 107, 108] films. It appears that specific microstructures including crystallinity, nature of the phases (anatase, rutile or both) and porosity which are determined by the processing conditions control the dielectric properties of the TiO_2 films [31].

Electrical conductivity of sprayed TiO_2 films

For the characterization of sprayed TiO_2 films we used the model of two capacitors (SiO_2 and TiO_2) connected in series (Fig. 3.14). Additional elements of the circuit such as 2 parallel resistors R1 and R2 and a series resistor R3 were included as well. In order to get the capacitance and resistance of TiO_2 layer we measured the impedance of the $Si/SiO_2/TiO_2$ structure at zero bias in the frequency range of 10Hz-1MHz. The AC voltage was chosen as 20 mV. The capasitance *vs.* frequency dependence was fitted by means of the above mentioned model (using freeware Zview2). The conductivity of TiO_2 layer was calculated from the fitting results at various measurement temperatures in the range of 20-200 °C.

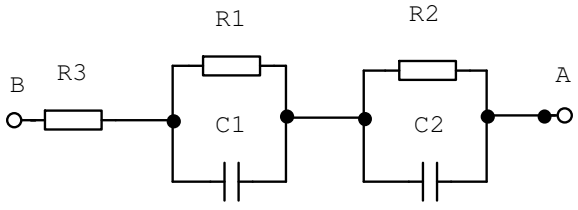

Figure 3.14. Equivalent circuit which best reproduces the frequency response of the $TiO_2/SiO_2/Si$ structure. C_1, C_2, R_1, R_2 are correspondingly the capacitance and resistance of TiO_2 and SiO_2 while R_3 is the resistance of the electrodes.

The obtained resistivity values for TiO_2-anatase and –rutile films were in order of 10^6 and 10^7 Ω·cm, respectively. For comparison, in the literature the reported electrical conductivity values for sprayed TiO_2-anatase films are in the order of 10^{-12} $\Omega^{-1}\cdot cm^{-1}$ [46]. Rasti and Brodie have shown that the resitivity values for sprayed TiO_2-anatase depend on the annealing atmosphere as the values in order of 10^{-6}, 10^{-8} and 10^{-9} Ω·cm were obtained when sample was annealed in O_2, air and vacuum, respectively [58]. The resistivity values for sprayed TiO_2-rutile in the range of $8\cdot10^6$ Ω·cm to $5\cdot10^8$ Ω·cm were detected [38]. The resitivity for sol-gel dip-coated TiO_2-anatase films is in order of 10^{10} up to 10^{11} Ω·cm [109].

The temperature dependence of the conductivity of TiO_2 films as a plot of lnσ *vs.* 1/T is presented in Figure 3.15. The thermal activation energy of conductivity (E_A) is approximately 101±5 meV in TiO_2-anatase and 63±5 meV in TiO_2-rutile films. Similar values are reported in literature [110, 111]. It is known that electrical conductivity of TiO_2 is determined by oxygen vacancies [58] and thus the conductivity activation energy can be assigned to this donor level.

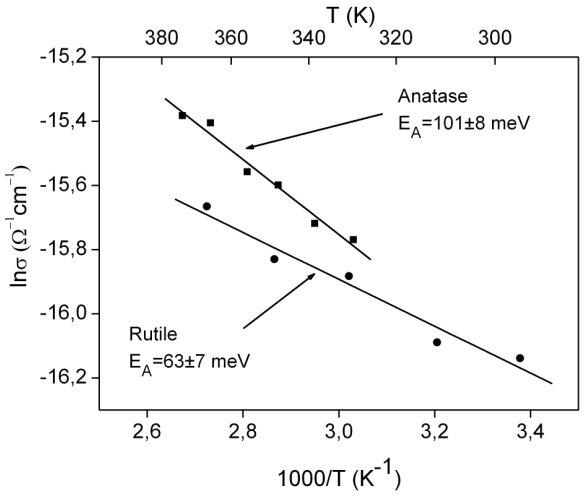

Figure 3.15. Temperature dependence of the conductivity of sol-gel sprayed TiO_2 films. E_A is the thermal activation energy of the conductivity.

In conclusion, our studies indicate that TiO_2 films with relatively high effective dielectric constant can be grown by spray pyrolysis. According to the calculated resistivity values the obtained TiO_2 films exhibit neither good dielectric nor semiconducting properties. On the other hand, the calculated thermal activation energy of conductivity indicates that these TiO_2 films have relatively good semiconducting properties. However, the semiconducting properties are determined not only by E_A but the concentration of donor defects should be considered as well.

3.3 Porous TiO_2 films by sol-gel method

Sol-gel derived porous TiO_2 films were deposited by the spin-coating and spray pyrolysis techniques. To obtain TiO_2 films with a porous structure PEG600 was added as a structure directing agent into the sol-gel solution containing acacH stabilized TTIP in EtOH (for details see Table 2.2 in section 2.2.1). The precursor solution for spin-coating deposition contained TTIP:acacH:EtOH in a molar ratio of 1:2:42 at TTIP concentration of 10.2 vol.% and the amount of PEG was varied in the range TTIP:PEG=1:0.25-7.7. Films were deposited at RT and subjected to the post-deposition annealing in the temperature region of 300-850 °C. In the case of spray pyrolysis deposition, the precursor solution containing TTIP:acacH:EtOH in molar ratio of 1:2:52 at TTIP concentration of 8.5 vol.% with TTIP:PEG=1:0.25-7.7 was sprayed onto the pre-heated substrate at T_S= 350 or 500 °C, followed by the annealing at 500 °C.
In this section, SEM results of the spin-coated and sprayed TiO_2 films are first reported, and morphological changes are characterized. After this, the structural development of TiO_2 films is presented according to XRD and FTIR studies. The results of structural and morphological studies on the formation of porous TiO_2 films by spin-coating and spray techniques are discussed in [V].

3.3.1 Morphology of porous TiO_2 films

SEM study

SEM microphotos were used to study the pore formation as well as to determine the grain size of the spin-coated and sprayed TiO_2 films [V].
As-sprayed TiO_2 films at T_S=500 °C contain pores and grains with diameters less than 10 nm. Upon annealing at 500 °C their size increases up to 10-20 nm according to SEM plain view micrographs (Fig.3.16). The SEM micrographs of the cross-section reveal an average pore size of approximately 20 nm in the as-deposited and 40 nm in the annealed film (Fig. 3.17). The grain size increases from 15 nm up to 25 nm. The thickness of the film was found to be approximately 2.3 μm after 50 spray pulses (10 s spray + 300 s pause).
Using spin-coating technique, TiO_2 films can be modified from smooth surface to a porous one simply by increasing the PEG concentration in the precursor solution (Fig. 3.18 (a-c), Table 3.4). TiO_2 films with the largest pore size were obtained when TTIP:PEG molar ratio in the precursor solution was 1:3.5 (Fig. 3.18 c, Table 3.4). A further increase in the amount of PEG was found to decrease the pore size (Fig. 3.18 d). According to the SEM cross-sectional micrographs the film thickness is approximately 120 nm.

Table 3.4. Grain and pore size evolution in spin-coated and spray deposited TiO_2 films as a function of PEG600 concentration in precursor solution

Method	Sol	TTIP:PEG600, molar ratio	Deposition temp, °C	T_{AN}, °C	Grain size, nm	Pore size, nm
Spray pyrolysis	TTIP:acacH:EtOH 1:2:52 (molar ratio) [TTIP]=8.5 vol.%	1:7.7	350	-	-	-
		1:7.7	350	500	-	-
		1:7.7	500	-	<10	<10
		1:7.7	500	500	10-20	10-20
Spin coating	TTIP:acacH:EtOH 1:2:42 (molar ratio) [TTIP]=10.2 vol.%	1:0.25	RT	450	15	7
		1:0.77	RT	450	15-25	10-15
		1:3.5	RT	450	35	25
		1:7.7	RT	450	<30	<20

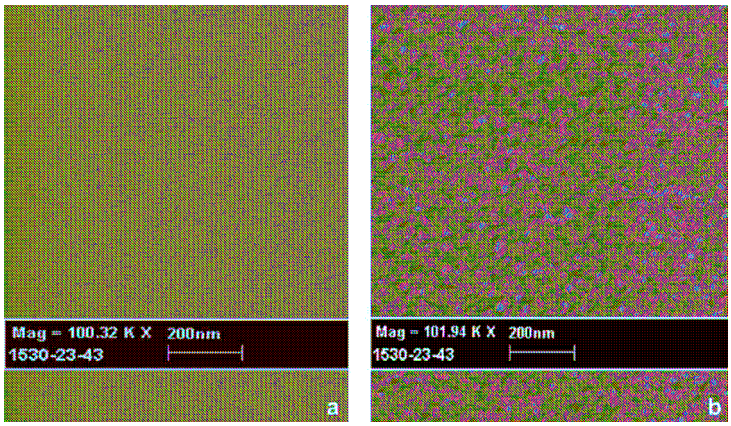

Figure 3.16. SEM micrographs of sprayed TiO_2 films prepared from a solution containing TTIP:PEG600 in a molar ratio of 1:7.7: (a) deposited at 500 °C; (b) deposited at 500 °C and annealed at 500 °C for 2 h in air.

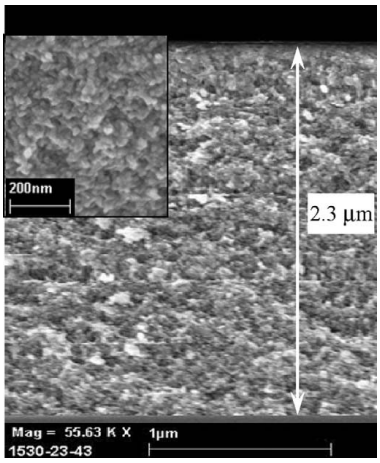

Figure 3.17. The cross-section of sprayed TiO_2 film prepared from a solution containing TTIP:PEG600 in a molar ratio of 1:7.7 (flat view shown in Fig. 3.16.b).

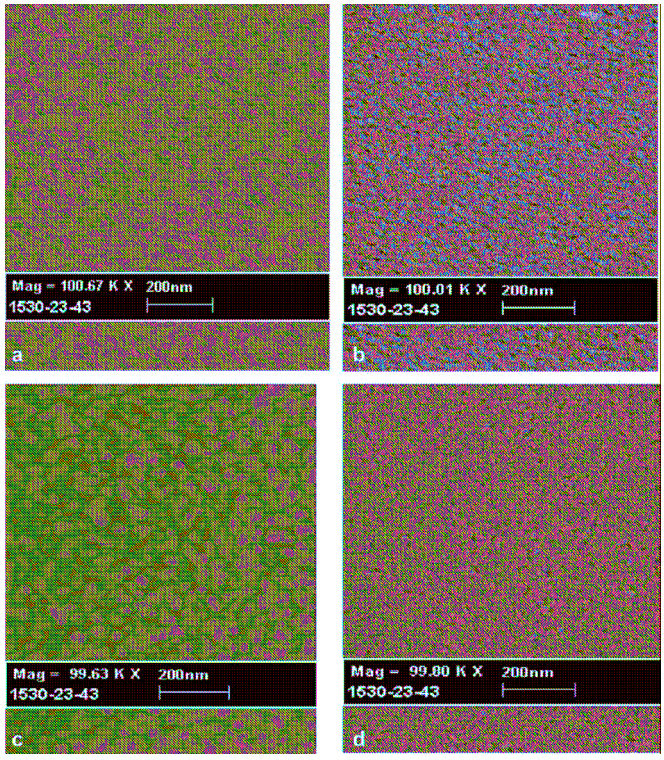

Figure 3.18. SEM micrographs of spin-coated TiO_2 films prepared with different TTIP:PEG600 molar ratios (a) 1:0.25, (b) 1:0.77, (c) 1:3.5, (d) 1:7.7 in solution. The films are annealed at 450 °C for 1 h in air.

3.3.2 Structural study of porous TiO_2 films

The structural development of porous TiO_2 films deposited by the spin-coating and spray pyrolysis techniques was characterized with the help of FTIR and XRD analysis [V].

FTIR study

The IR spectra of TiO_2 films deposited either by spray pyrolysis or spin-coating are presented in Figs 3.19 and 3.20. The strong absorption bands close to 2875 and 1120 cm^{-1} in the spin-coated film dried at 100 °C (Fig. 3.20) and sprayed film at T_S=350 °C can be assigned to the C-H [66] and CH_2-O-CH_2 [68] vibrations of PEG, respectively. TiO_2 films deposited by spray pyrolysis at substrate temperature of 350 °C (from precursor solutions with TTIP:PEG=1:7.7) still contain organic compounds (Fig. 3.19). Only upon the deposition or annealing at 500 °C TiO_2 films free of organic residues were obtained. In addition, at this temperature the formation of anatase Ti-O-Ti bonds (around 440 cm^{-1}) could be observed. Post-deposition annealing at 500 °C for 2 h in air determines the sharpness of this absorption band (Fig. 3.19).

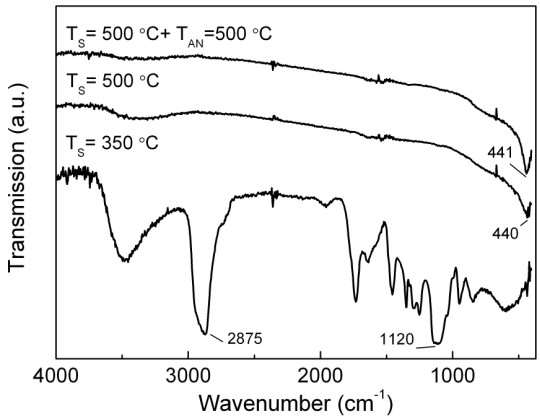

Figure 3.19. FTIR spectra of sprayed TiO_2 films deposited from a solution containing TTIP:PEG600 in a molar ratio of 1:7.7 at substrate temperatures (T_S) of 350 and 500 °C; and a spectrum of the film deposited at 500 °C and additionally annealed (T_{AN}) at 500 °C.

In the case of spin-coating TiO_2 films (Fig. 3.20), annealing temperature of at least 300 °C is needed to completely remove PEG from the film. Annealing above 400 °C promotes the formation of TiO_2-anatase, as confirmed by the appearance of the peak around 430 cm^{-1} [96].

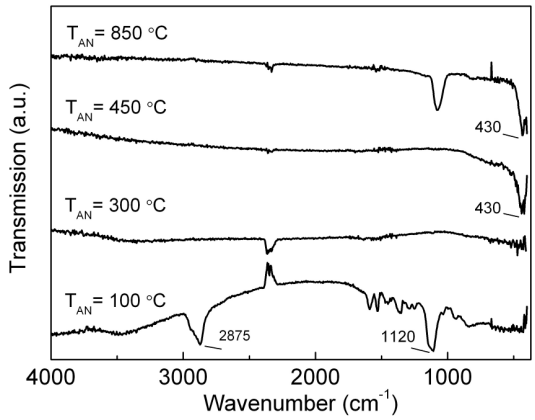

Figure 3.20. FTIR spectra of TiO_2 films, prepared by the spin-coating technique from a solution containing TTIP:PEG600 in a molar ratio of 1:0.25, and annealed at different temperatures for 1 h.

XRD study

According to XRD studies, crystalline TiO_2 anatase films deposited by spin-coating are obtained only upon annealing at temperatures above 700 °C [VI].

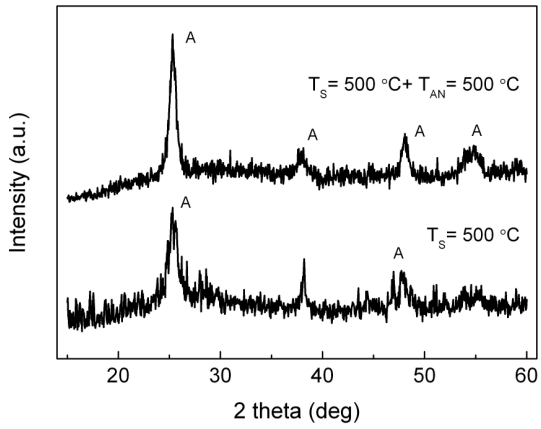

Figure 3.21. XRD patterns of sprayed TiO_2 films deposited from a solution containing TTIP:PEG600 in a molar ratio of 1:7.7 at substrate temperature (T_S) of 500 °C and of the film additionally annealed (T_{AN}) at 500 °C for 2 h in air.

Using spray deposition, TiO_2 films deposited at T_S< 500 °C are amorphous but the as-sprayed films grown at T_S= 500 °C (Fig. 3.21) show a broad peak at 2θ= 25° which belongs to the anatase phase (JCPDS-PDF 21-1272). Post-deposition

annealing at 500 °C leads to the sharpening of the diffraction peaks characteristic of anatase (Fig. 3.21). Crystallite sizes calculated from the XRD patterns using the Scherrer formula are 5 nm and 9 nm in the as-deposited and at 500 °C annealed film, respectively

Our results on spin-coated films are similar to those reported in the literature, where TiO_2 films free of organics could be obtained after annealing at 300 °C [68] and pore size can be varied by increasing either the molecular weight or molecular mass of PEG [68]. To our knowledge no results are published on porous TiO_2 films deposited by spray pyrolysis from solutions containing PEG. However, the porous structure formation as a function of the solvent used has been reported in several studies [51, 53], *e.g.* structured TiO_2 films derived from Ti-powders in H_2O_2 and NH_4OH have found to indicate open pore structure with a pore size of 1-2 μm [55].

In conclusion, iff appears established that, according to the morphological and structural studies, porous TiO_2 films can be deposited by spin-coating and spray pyrolysis techniques by adding PEG in the precursor solution.

3.4 Performance of eta-type solar cell on sol-gel derived TiO_2 window layer

This part of the research work was done at Hahn-Meitner Institute (HMI) Berlin. In my thesis I shall give a short overview of some output characteristics of the eta-type solar cell (TiO_2/$In(OH)_xS_y$/PbS(O)/PEDOT:PSS) were $In(OH)_xS_y$ and PbS(O) layers are deposited by the SILAR technique onto sol-gel derived porous TiO_2 layers. It should be mentioned that even though in eta-solar cell TiO_2 layers (flat and porous) are deposited by sol-gel dip-coating technique no direct connection with the results reported on sol-gel spin-coating or spray pyrolysis deposited TiO_2 films (see sections 3.2 and 3.3) should be derived. Moreover, obtained porosity for the spin-coated and sprayed TiO_2 films is probably too low in order to use it as a window layer in this type of solar cell structures where PEDOT:PSS is used as a hole conductor.

In the previous studies, by the same group at HMI it has been demonstrated that the TiO_2/$In(OH)_xS_y$/PbS(O)/PEDOT:PSS system is suitable for photovoltaic applications [80]. In that study solar cell structure was deposited onto sprayed porous TiO_2 layer. As the method used to grow porous TiO_2 by spray pyrolysis, as reported in reference [80], was rather sophisticated new routes were applied for the porous TiO_2 film deposition. Sol-gel dip-coating seemed to be a reasonable method as by this method the structure of the film can easily be modified by changing the withdrawal speed of the sample from the precursor solution [67].

Also in comparison with the earlier studies where $In(OH)_xS_y$ and PbS(O) layers were deposited by chemical bath (CBD) method [80] this time [VI] SILAR technique was applied which exploits the successive adsorption of metal ions and their reaction with sulfur ions [112]. In comparison to CBD, the SILAR technique can be very precisely controlled and deposition conformal to the substrate takes place.

The main emphasis in this part of the work is to optimize of the solar cell structures for a given morphology of TiO_2 by varying the thickness and the annealing conditions of the $In(OH)_xS_y$ and PbS(O) layers as well as by introducing a Nb doped TiO_2 layer into the solar cell structure. The results reported in more detail can be found in [VI].

Approach to eta-solar cell deposition

Our attempt to optimize the $TiO_2/In(OH)_xS_y$/PbS(O)/PEDOT:PSS solar-cell structure is based on varying systematically the annealing temperature (T_{AN}) and the thickness of $In(OH)_xS_y$ (20-40 coating cycles, T_{AN}= RT-350 °C) and PbS(O) (5-25 coating cycles, T_{AN}= RT-250 °C) layers. It is known from literature that the thickness of the film deposited by SILAR is directly controlled by the number of deposition cycles [112-114]. For a detailed description of the deposition of $In(OH)_xS_y$ and PbS(O) layers and the whole solar cell preparation, see section 2.3.1 It should be mentioned here that for variation of the thicknesses of the PbS(O) or $In(OH)_xS_y$ layers, the thicknesses of the $In(OH)_xS_y$ or PbS(O) layers were kept constant (35 or 15 dips, respectively). Besides, the properties of the porous TiO_2 layer were kept constant in all experiments performed.

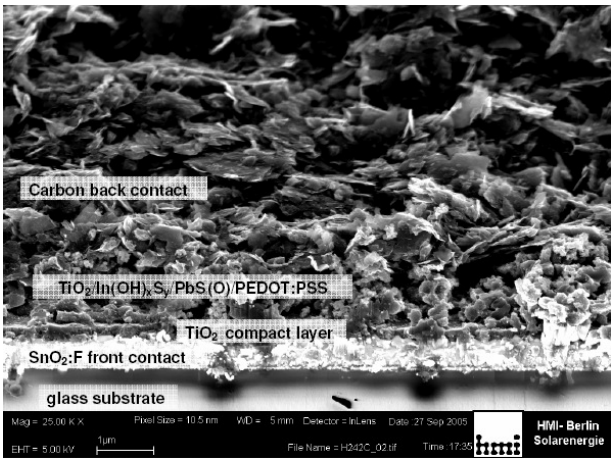

Figure 3.22. Cross-sectional view by SEM of a solar-cell structure consisting of a SnO_2:F front contact, a TiO_2 compact layer, a $TiO_2/In(OH)_xS_y$/PbS(O)/PEDOT:PSS layer and the carbon back contact. The sample is tilted by 30◦ towards the surface.

Figure 3.22 shows a typical solar-cell structure consisting of a SnO_2:F front contact, a TiO_2 compact layer, a $TiO_2/In(OH)_xS_y$/PbS(O)/PEDOT:PSS layer and a carbon back contact. The SnO_2:F and TiO_2 flat layers can be clearly distinguished while the $TiO_2/In(OH)_xS_y$/PbS(O)/PEDOT:PSS layer looks more like an agglomerate in the SEM picture. The carbon particles are like flat plates with a diameter in the order of several 100 nm, contacted to the PEDOT:PSS.

Optimization potential

For a given morphology of the porous TiO_2, the values of V_{OC} and I_{SC} may be optimized by variation of the thicknesses of the PbS(O) and $In(OH)_xS_y$ layers (Fig. 3.23). With an increasing thickness of the PbS(O) layer from five to ten dips, both V_{OC} and I_{SC} increase while for thicknesses larger than 15 dips V_{OC} and j_{SC} decrease. With an increasing thickness of the $In(OH)_xS_y$ layer, j_{SC} monotonously increases whereas V_{OC} decreases. The decrease in V_{OC} becomes more pronounced for an increasing thickness of the $In(OH)_xS_y$ layer from 35 to 40 dips on wards.

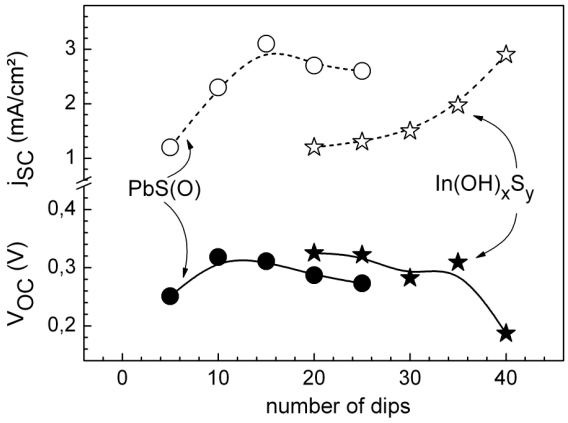

Figure 3.23. Dependence of the short circuit current (open symbols) and of the open circuit voltage (filled symbols) on the thickness of the $In(OH)_xS_y$ (stars) and of the PbS (circles) layers in SnO_2:F/TiO_2/ $In(OH)_xS_y$ /PbS(O)/PEDOT:PSS/C structures. The thickness is given as the number of SILAR-dip cycles.

With an increasing annealing temperature of $In(OH)_xS_y$, the open circuit voltage (V_{OC}) monotonously decreases from more than 0.6 V to less than 0.2 V while the values of the short circuit current density (j_{SC}) increase from about 0.2 mA/cm^2 to about 4 mA/cm^2. The annealing temperature of PbS(O) does not significantly influence V_{OC}, and j_{SC} starts to decrease at annealing temperatures of PbS(O) above 250 °C.

The (local) thickness of the PbS(O) and $In(OH)_xS_y$ layers cannot be changed in a wide range as demonstrated above. Incidentally, the samples were opaque after the deposition of the $In(OH)_xS_y$ and PbS(O) layers. Therefore, the output parameters of the solar cell do not only depend on the properties of $In(OH)_xS_y$ and PbS(O) layers. Primarily, the morphology of the TiO_2 layer has to be improved in such a manner that the internal surface area increases by a factor of 5-10 in comparison to the substrates used in this work. By this way, the amount of absorbing material will be increased. At the same time, the back contact has to be intimate to the absorber in all structures. This implements the need for pore sizes of the order of 100 nm or more and a good penetration of the hole conducting PEDOT:PSS.

Another way for optimizing the performance of SnO_2:F/TiO_2/$In(OH)_xS_y$/PbS(O)/ PEDOT:PSS/C structures is to modify the TiO_2, for example by Nb doping. The largest short circuit current (10.2 mA/cm^2) was reached with Nb-doped TiO_2. However, the value of V_{OC} was only 0.17 V. The efficiency of solar energy conversion is about 1% for this structure.

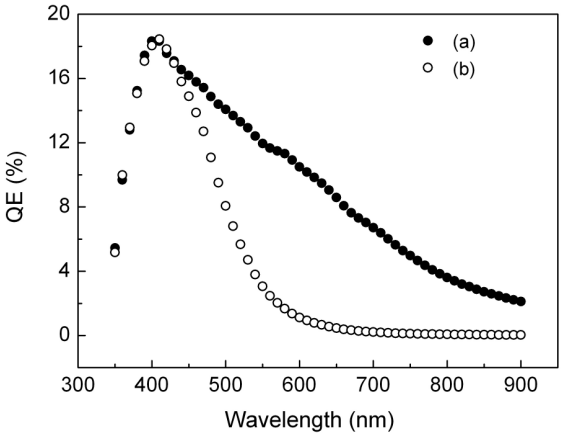

Figure 3.24. Spectral dependence of the quantum efficiency of (a) SnO_2:F/TiO_2/$In(OH)_xS_y$ /PbS(O)/PEDOT:PSS/C and (b) SnO_2:F/TiO_2/TiO_2:Nb/ $In(OH)_xS_y$ /PbS(O)/PEDOT:PSS/C structures.

Figure 3.24 shows the spectral dependence of the quantum efficiency for a solar cell structure with and without TiO_2:Nb layer. The values of QE are in general not high (in the order of 10-20 %) what is mostly related to the partial transparency of the layer. For the solar cell structure with TiO_2:Nb, QE is much larger in the region of longer wavelengths than for solar cell structures without Nb. This effect obviously means that the charge generated in the PbS(O) layer can reach the contacts when the solar cell structure with Nb doped TiO_2 layer is used.

In conclusion, structures of TiO_2/$In(OH)_xS_y$/PbS(O)/PEDOT:PSS were entirely prepared by non-vacuum and low-temperature processes. It has been shown that the photoelectrical properties of TiO_2/$In(OH)_xS_y$/PbS(O)/PEDOT:PSS structures are determined by the annealing temperature of $In(OH)_xS_y$ in air. Moreover, the morphology and doping of the TiO_2 layers are also extremely important for a significant improvement of the solar cell performance for the adopted configuration of the TiO_2/$In(OH)_xS_y$/PbS(O)/PEDOT:PSS structure where an efficiency of 3-5% seems to be realistic.

CONCLUSIONS

1. Thermal degradation of titanium(IV) acetylacetonate xerogels, obtained from the solution containing titanium(IV) tetraisopropoxide and acetylacetone at molar ratios of 1:1 (Ti-1) and 1:2 (Ti-2) in 2-methoxyethanol was monitored in the temperature range of 30-700 ºC. Thermal degradation of Ti-1 and Ti-2 consists of 6 mass loss steps with the total mass loss of 46.3 % and 54.4 %, respectively. The solid residues from 700 °C in air show rutile to anatase contents in an approximate ratio of 72:28 and 26:74 for Ti-1 and Ti-2, respectively. The samples release only water up to 120 ºC. In the temperature region of 120-320 ºC, the main evolved gases were acetone, acetic acid as well as a gaseous species with *m/z*= 74 which were released from both precursors, while acetylacetone evolved from Ti-2 only. Continuous evolution of CO_2 and H_2O is detected up to the end of the decomposition of Ti-1 and Ti-2 at approximately 550°C.

2. Phase composition and crystallinity of sol-gel spray deposited TiO_2 films, grown from solution containing titanium(IV) tetraisopropoxide, acetylacetone and ethanol, are controlled by both deposition and annealing temperatures. As-deposited films grown at T_S<500 °C are amorphous but crystalline films could be obtained by deposition at 500 °C or by post-deposition annealing at 500 °C and above. Annealing at 700 and 800 °C results in a mixture of anatase and rutile or rutile if grown at T_S=435 °C or 500 °C, respectively, whereas the films grown at T_S<400 °C remain anatase. Sprayed TiO_2 films show surface roughness below 1 nm, refractive indices of 2.1-2.3 and 2.6 and effective dielectric constant values between 36-46 and 53-70 for the anatase and rutile phases, respectively.

3. It is shown that nanoporous TiO_2 films with a pore size up to 30-40 nm can be deposited by sol-gel spray pyrolysis and spin-coating methods from the precursor solution containing polyethylene glycol. Crystalline TiO_2-anatase films could be grown by spray pyrolysis at T_S=500 °C whereas in the case of spin-coating, post-deposition annealing at temperatures in the order of 700 °C is needed.

4. It is shown that the photoelectrical properties of TiO_2/$In(OH)_xS_y$/ PbS(O)/PEDOT:PSS structures are controlled by the number of SILAR cycles and the annealing temperature of $In(OH)_xS_y$. An improvement of the solar cell performance could be obtained using a Nb doped TiO_2 layer in the TiO_2/$In(OH)_xS_y$/PbS(O)/PEDOT:PSS system.

ACKNOWLEDGEMENTS

I am very much indebted to my supervisor, Research Professor Malle Krunks, for her support, advice and encouragement over the years and for believing in me.

I would like to thank Head of the Department Prof. Enn Mellikov for giving me the opportunity to carry out my studies in the Department of Materials Science at Tallinn University of Technology.

My deepest gratitude belongs to my co-author Prof. Lauri Niinistö for his continuous support and fruitful discussions throughout writing process of the thesis.

I would also like to thank each colleague, former and present, at the Department of Materials Science, for the pleasant working atmosphere and co-operation. It has been most pleasant to work with all of you. My special thanks belong to my colleagues in thin films group and co-authors; senior researcher A. Mere is thanked for explaining me patiently the world of physics and senior researcher K. Tõnsuaadu is thanked for the thermal analysis measurements.

I have had pleasant and fruitful collaboration with several people in different research groups. Special thanks to Prof. M. Es-Souni, C.-H. Solterbeck, A. Piorra and Dr. S. Jakovlev in IMST at Kiel University of Applied Sciences for the introduction to the sol-gel processing and dielectric materials. I would also like to thank Prof. A. Goossenss and Dr. M. Nanu for the opportunity to perform Raman spectroscopy measurements at Delft University of Technology. Many thanks are also due to Dr. Th. Dittrich, T. Guminskaja, Dr. A. Belaidi and Dr. L. Dlozcik at HMI for the opportunity to carry out part of the work together with them and to gain knowledge about eta-solar cell. Special thanks to Dr. J. Madarácz for EGA-MS measurements and fruitful discussions during the paper writing process as well as for the pleasant stay in Budapest.
Financial support from Estonian Science Foundation grants 5612 and 6954, German Federal Ministry of Education and Research (BMBF) under the WTZ project EST 02/001, European Commission RTN-project HRNP-CT-2000-00101, EU FP5 project ENK6-CT-2002-80664, Deutsche Bundesstiftung Umwelt (DBU), Estonian Doctoral School of Materials Science and Materials Technology (MMTDK) are gratefully acknowledged.

My warmest gratitude belongs to my family.

Tallinn, June 2007

Ilona Oja Açik

ABSTRACT

Sol-Gel Deposition of Titanium Dioxide Films

This study focuses on the sol-gel derived TiO_2 films deposited by spray pyrolysis and spin-coating techniques as was well as on the film formation process as monitored by thermal analysis measurements.

In order to find the proper temperature profile for TiO_2 film deposition, comprehensive thermal analyses (TG/DTG/DTA coupled with EGA-FTIR and MS) were conducted on dried TiO_2-gel powders, derived from the precursor system containing titanium(IV) tetraisopropoxide, acetylacetone and 2-methoxyethanol at Ti-source to acetylacetone molar ratios of 1:1 (Ti-1) or 1:2 (Ti-2). Elemental, FTIR and XRD analyses where used to characterize the dried gels, intermediates as well as the final products of thermal decomposition. Thermal degradation of the Ti-1 and Ti-2 dried gel powders in the temperature range of 30-700 ºC consists of 6 mass loss steps with the total mass loss of 46.3 % and 54.4 %, respectively. The samples release only water up to 120 ºC. The further decomposition steps up to 550 °C are exothermic and include the evolution of CO_2 and H_2O. In the temperature region of 120-320 ºC, the main released gases were acetone and acetic acid, released from both precursors as well as acetylacetone evolved from Ti-2 only, as shown by both EGA-FTIR and EGA-MS. According to XRD, the solid residues from 700 °C in air show rutile to anatase approximate ratio of 72:28 and 26:74 for Ti-1 and Ti-2, respectively.

Sol-gel derived flat TiO_2 films were deposited by the spray pyrolysis technique from the precursor system containing titanium(IV) tetraisopropoxide, acetylacetone and ethanol. A comprehensive investigation into the structural, morphological, optical and electrical properties of flat TiO_2 films was performed with the help of FTIR, XRD, Raman, AFM, ellipsometry and impedance spectroscopy measurements. According to the FTIR, XRD and Raman measurements as-deposited flat TiO_2 films grown by spray pyrolysis at $T_S < 500$°C are amorphous. Only the deposition or annealing at 500 °C results in films with anatase phase and free of contaminants. Annealing at $T_{AN} \geq 700$°C leads to crystalline anatase if films are deposited at $T_S < 400$°C whereas the films grown either at $T_S = 435$°C or 500°C consist of a mixture of anatase-rutile or rutile, respectively. TiO_2-anatase films show refractive indices between 2.1 and 2.3 and an rms roughness between 0.35 and 0.70 nm while for TiO_2-rutile films the values are 2.6 and 0.70 nm, respectively. TiO_2-anatase and –rutile films show at 10 kHz dielectric constant values of 36-46 and 53-70, respectively.

In order to obtain porous TiO_2 films by the spray pyrolysis and spin-coating techniques, polyethylene glycol as a structure directing agent was added into the solution. According to SEM relatively well-adherent TiO_2 films with pore sizes up

to 40 nm and 30 nm could be deposited from used precursor solutions by spray pyrolysis and spin-coating methods, respectively. XRD studies revealed that crystalline porous TiO_2-anatase films could be grown by spray pyrolysis at T_S= 500°C whereas in the case of spin-coating, a post-deposition annealing at temperatures in order of 700 °C is needed.

An attempt to optimize the eta-solar cell structures $TiO_2/In(OH_x)S_y/PbS(O)/$ PEDOT:PSS deposited onto a sol-gel derived porous TiO_2 layer is performed by SEM, I-V and QE measurements. A significant improvement of the solar cell performance was detected when Nb doped TiO_2 layer was used in the $TiO_2/In(OH)_xS_y/PbS(O)/PEDOT:PSS$ system.

KOKKUVÕTE

Titaandioksiidi kiled sool-geeli meetodil

Antud töös on käsitletud TiO_2 moodustumist sool-geeli protsessis ning sool-geeli pihustuspürolüüsi või pindvurritamise meetodil valmistatud TiO_2 kilede omadusi.

Doktoritöös uuriti kahe titaan(IV) atsetüülatsetonaadi kuivatatud geeli termilist lagunemist õhu keskkonnas, rakendades termoanalüütiliste meetodite kompleksi (TG/DTG/DTA koos EGA-FTIR ja EGA-MS analüüsidega). Geelid saadi titaan(IV) isopropoksiidi, atsetüülatsetooni ja 2-metoksüetanooli sisaldavatest lähtelahustest, kus Ti-allika ja atsetüülatsetooni molaarsuhe oli 1:1 (Ti-1) ja 1:2 (Ti-2). Ti-1 ja Ti-2 kserogeelide termiline lagunemine temperatuuridel 30-700ºC koosneb kuuest massikao etapist summaarse massikaoga vastavalt 46.3 ja 54.4%. TG analüüsi kohaselt on lagunemine praktiliselt lõppenud ligikaudu 550ºC juures. Mõlema kserogeeli korral on H_2O peamine gaasifaasiline laguprodukt kuumutamisel kuni 120ºC-ni. Järgmised lagunemisetapid kuni 550°C-ni on eksotermilised - jätkub H_2O eraldumine sünkroonselt CO_2-ga. Temperatuuridel 120-320ºC on peamisteks eralduvateks gaasideks atsetoon, äädikhape ja gaas millele on iseloomulik *m/z*= 76 ning atsetüülatsetoon, kusjuures neist viimane eraldub ainult Ti-2-st. XRD järgi koosneb termogravimeetrilise analüüsi lõpp-produkt 700°C juures rutiili ja anataasi faaside segust nende ligikaudse kvantitatiivse suhtega 72:28 (Ti-1) ja 26:74 (Ti-2).

Sool-geel pihustuspürolüüsi meetodil sadestatud TiO_2 kilede valmistamisel kasutati titaan(IV) isopropoksiidi, atsetüülatsetooni ja etanooli sisaldavat lähtelahust. Moodustunud TiO_2 kilede struktuuri, morfoloogiat, optilisi ning elektrilisi omadusi uuriti sõltuvalt kilede sadestus- ja järeltöötluse temperatuuridest, kasutades FTIR, XRD, Raman, AFM, ellipsomeetria ja impedants spektroskoopia meetodeid. Uurimistöö tulemused näitasid, et TiO_2 kilede struktuursed omadused on olulisel

määral kontrollitavad sadestustemperatuuriga. Temperatuuridel 300-450°C sadestatud kiled on röntgenamorfsed. Orgaanilistest jääkproduktidest vabad, kristallilised, anataasi struktuuriga kiled saadakse kasvatamisel 500°C juures. Temperatuuridel kuni 400°C pihustatud kiled on anataasi struktuuriga ka pärast kuumutamist 800°C juures. Kiled sisaldavad rutiili faasi kui kasvatada temperatuuridel T> 400°C ja kuumutada 700°C juures. Anataasi struktuuriga TiO_2 kilede murdumisnäitaja ja pinnakareduse väärtused on vastavalt vahemikus 2.1-2.3 ja 0.35-0.70 nm, rutiili struktuuri puhul on nende väärtused vastavalt 2.6 ja 0.7 nm. TiO_2 kilede suhteline dielektriline konstant on anataasi struktuuri korral vahemikus 36-46 ja rutiili struktuuri puhul 53-70.

Poorsete TiO_2 kilede valmistamiseks lisati lähtelahusesse polüetüleenglükooli kui pooritekitajat. Poorsed kiled sadestati nii pihustamise kui pindvurritamise tehnikatega. Saadud TiO_2 kilesid iseloomustati SEM, FTIR ja XRD analüüsi meetoditel. SEM-i tulemustest lähtuvalt on võimalik pihustuspürolüüsi ja pindvurritamise meetoditel valmistada hea adhesiooniga nanokristallilised nanopoorsed (pooride suurus 30-40 nm) TiO_2 kiled. Pihustuspürolüüsi korral saadakse nanopoorsed kristallilised TiO_2-anataas kiled sadestamisel 500°C juures. Kasutades pindvurritamise tehnikat, on kristalliliste TiO_2-anataas kilede saamiseks vajalik täiendav kuumutamine vähemalt 700°C juures.

Eta-tüüpi fotovoltstruktuur $TiO_2/In(OH_x)S_y/PbS(O)/PEDOT:PSS$ sadestati SILAR tehnikaga eelnevalt sool-geeli meetodil valmistatud poorsele TiO_2 kihile. Struktuuri optimiseerimise võimalikke tehnoloogilisi viise iseloomustati SEM, I-V ja QE mõõtmiste kaudu. Leiti, et lisaks $In(OH_x)S_y$ kihi tehnoloogia optimeerimisele aitab fotovoltstruktuuri kõrgemaid väljundparameetreid saavutada Nb-ga legeeritud TiO_2 kihi kasutamine $TiO_2/In(OH_x)S_y/PbS(O)/PEDOT:PSS$ struktuuris.

REFERENCES

1. A.I. Kingon, J.-P. Maria, S.K. Streiffer, *Nature* 406 (2000) 1032-1038.
2. M. Grätzel, *Nature* 414 (2001) 338-334.
3. M. Okuya, K. Nakade, D. Osa, T. Nakano, G.R. Asoka Kumara and S. Kaneko, *J. Photochem. Photobiol. A: Chem.* 164 (2004) 167-172.
4. U. Schubert, *J. Chem. Soc., Dalton Trans.* (1996) 3343-3348.
5. O. Carp, C.L. Huisman, A. Reller, *Progr. Solid State Chem.* 32 (2004) 33-177.
6. A. Yimit, A.G. Rossberg, T. Amemiya, K. Itoh, *Talanta* 65 (2005) 1102-1109.
7. J. Livage, D. Ganguli, *Sol. Energ. Mater. Sol. Cell. 68* (2001)365-381.
8. R.M. Wallace, *Appl. Surf. Sci.* 231-232 (2004) 543-551.
9. S.A. Campbell, H.-S. Kim, D.C. Gilmer, B. He, T. Ma, W.L. Gladfelter, *IBM J. Res. Develop.,* 43 (1999) 383-392.
10. G.K. Mor, O.K. Varghese, M. Paulose, K. Shankar, C.A. Grimes, *Sol. Energ. Mater. Sol. Cell. 90 (2006) 2011-2075.*
11. B. O'Regan, M. Grätzel, *Nature* 353 (1991) 737-740.
12. I. Kaiser, K. Ernst, Ch.-H. Fischer, R. Könenkamp, C. Rost, I. Sieber, M. Ch. Lux-Steiner, *Sol. Energ. Mater. Sol. Cell.* 67 (2001) 89-96.
13. P.T. Moseley, *Meas. Sci. Technol.* 8 (1997) 223-237.
14. F.H. Jones, *Surf. Sci. Rep.* 42 (2001) 75-205.
15. K.J. Hadjiivanov, D.G. Kissurski, *Chem. Soc. Rev*. 25 (1996) 61-69.
16. A.J. Moulson, J.M. Herbert, 1991, *Electroceramics: Materials Properties and Applications*, Chapman and Hall, London, 226
17. V. Sammelselg, A. Rosental, A. Tarre, L. Niinistö, K. Heiskanen, K. Ilmonen, L.-S. Johansson, T. Uustare, *Appl. Surf. Sci.* 134 (1998) 78-86.
18. M. Ritala, M. Leskelä, L. Niinistö, P. Haussalo, *Chem. Mater.* 5 (1993) 1174-1181.
19. M. Ritala, M. Leskelä, E. Nykänen, P. Soininen, L. Niinistö, *Thin Solid Films* 225 (1993) 288-295
20. A.C. Pierre, 1998, *Introduction to sol-gel processing*, Kluwer Academic publishers, London, 1-9.
21. J. Livage, M. Henry, C. Sanchez, *Prog. Solid St. Chem*. 18 (1988) 259-341.
22. C.J. Brinker, G.W. Scherer, 1990, *Sol-gel science: the physics and chemistry of sol-gel processing*, Academic Press, Boston, 912 pages
23. U. Schubert, *J. Mater. Chem*. 15 (2005) 3701-3715.
24. C. Sanchez, J. Livage, M. Henry, F. Babonneau, *J. Non-Cryst. Solids* 100 (1988) 65-76.
25. M. Pathak, R. Bohra, R.C. Mehotra, I.-P. Lorenz, H. Piotrowski, *Transition Met. Chem*., 28 (2003) 187-192.
26. M. Sedlar, M. Sayer, *J. Sol-Gel Sci. Technol.* 5 (1995) 27-40.
27. W. Beier, A.A. Göktas, G.H. Frischat, *J. Non-Cryst. Solids* 121 (1990) 163-166.

28. R. Campostrini, M. Ischia, L. Palmisano, *J. Therm. Anal. Cal.* 71 (2003) 997-1009.
29. E.J.A. Pope. J.D. Mackenzie, *J. Non-Cryst. Solids* 87 (1986) 185-198.
30. J.-H. Yang, Y.-S. Han, J.-H. Choy, *Thin Solid Films* 495 (2006) 266-271.
31. M. Es-Souni, I. Oja, M. Krunks, *J. Mater. Sci. Mater. Electron.* 15 (2004) 341-344.
32. I. Oja, "*TiO_2 thin films by sol-gel process*" (2003), Thesis of Master of Science degree, Tallinn University of Technology, 96 pages.
33. A. Leaustic, F. Babonneau, J. Livage, *Chem. Mater.* 1 (1989) 240-247.
34. R.J. Errington, J. Ridland, W. Clegg, R.A. Coxall, J.M. Sherwood, *Polyhedron*, 17 (1998) 659-674.
35. B. Guo, Z. Liu, L. Hong, H. Jiang, *Surf. Coating Technol.* 198 (2005) 24-29.
36. Y. Ohya, J. Mishina, T. Matsuda, T. Ban, Y. Takahashi, *J. Am. Ceram. Soc*. 82 (1999) 2601-2606.
37. J. Madarász, M. Okuya, P.P. Varga, S. Kaneko, G. Pokol, *J. Anal. Appl. Pyrol.* 79 (2007) 479-483.
38. H.P. Deshmukh, P.S. Shinde, P.S. Patil, *Mater. Sci. Eng. B*, 130 (2006) 220-227.
39. A. Verma, S.B. Samanta, A.K. Bakhshi, S.A. Agnihotry, *Sol. Energ. Mater. Sol. Cell.* 88 (2005) 47-64.
40. R. Campostrini, M. Ischia, L. Palmisano, *J. Therm. Anal. Cal.* 71 (2003) 1011-1021.
41. R. Campostrini, M. Ischia, L. Palmisano, *J. Therm. Anal. Cal.* 75 (2004) 13-24.
42. R. Campostrini, M. Ischia, L. Palmisano, *J. Therm. Anal. Cal.* 75 (2004) 25-34.
43. P.S. Patil, *Mater. Chem. Phys.* 59 (1999) 185-198
44. J.B. Mooney, S.B. Radding, *Annu. Rev. Mater. Sci*. 12 (1982) 81-101.
45. O. Kijatkina "*Deposition of Copper Indium Disulphide Films by Chemical Spray Pyrolysis*", (2004), Thesis on Natural and Exact Sciences B28, Tallinn University of Technology, 132 pages.
46. L. Castañeda, J.C. Alonso, A. Ortiz, E. Andrade, J.M. Saniger, J.G. Bañuelos, *Mater. Chem. Phys.* 77(2002) 938-944.
47. A. Conde-Gallardo, M. Guerrero, N. Castillo, A.B. Soto, R. Fragoso, J.G. Cabaňas-Moreno, *Thin Solid Films* 473 (2005) 68-73.
48. M.O. Abou-Helal, W. T. Seeber, *Appl. Surf. Sci.* 195 (2002) 53-62.
49. A.I. Martínez, D.R. Acosta, A.A. López, *J. Phys. Condens. Matter.* 16 (2004) S2335-S2334.
50. C.H. Chen, E.M. Kelder, J. Schoonman, *Thin Solid Films* 342 (1999) 35-41.
51. M. Okuya, K. Shiozaki, N. Horikawa, T. Kosugi, G.R. Asoka Kumara, J. Madarász, S. Kaneko, G. Pokol, *Solid State Ionics* 172 (2004) 527-531.

52. A.M. More, J.L. Gunjkar, C.D. Lokhande, R.S. Mane, S-H. Han, *Micron* (2007), available online at www.sciencedirect.com
53. M. Okuya, N.A. Prokudina, K. Mushika, S. Kaneko, *J. Eur. Ceram. Soc.* 19 (1999) 903-906.
54. L. Kavan, M. Grätzel, *Electrochim. Acta* 40 (1995) 643-652.
55. N. Golego, S.A. Studenikin, M. Cocivera, *J. Mater. Res*. 14 (1999) 698-707.
56. K.D. Rogers, D.W. Lane, J.D. Painter, A. Chapman, *Thin Solid Films* 466 (2004) 97-102.
57. C. Natarajan, N. Fukunaga, G. Nogami, *Thin Solid Films* 322 (1998) 6-8.
58. M.A. Rashti, D. E. Brodie, *Thin Solid Films* 240 (1994) 163-167.
59. W. Que, A. Uddin, X. Hu, *J. Power. Sourc.* 159 (2006) 353-356.
60. U. Selvaraj, A.V. Prasadarao, S. Komarneni, R. Roy, *J. Am. Ceram. Soc*. 75 (1992) 1167-1170.
61. R. Fretwell, P. Douglas, *J. Photochem. Photobiol. Chem.* 143 (2001) 229-240.
62. A.K. Hassan, N.B. Chaure, A.K. Ray, A.V. Nabok, S. Habesch, *J. Phys. Appl. Phys*. 36 (2003) 1120-1125.
63. K.A. Vorotilov, E.V. Orlova, V.I. Petrovsky, *Thin Solid Films* 207 (1992) 180-184.
64. J.L. Keddie, P.V. Braun, E.P. Giannelis, *J. Am. Ceram. Soc.* 77 (1994) 1592-1596.
65. K.R. Patil, S.D. Sathaye, Y.B. Khollam, S.B. Deshpande, N.R. Pawaskar and A. B. Mandale, *Mater. Lett.* 57 (2003) 1775-1780.
66. Y. Djaoued, Simona Badilescu, P.V. Ashrit, D. Bersani, P.P. Lottici and R. Brüning, *J. Sol-Gel Sci. Technol.* 24 (2002) 247-254.
67. K. Kajihara, T. Yao, *J. Sol-Gel Sci. Technol.* 12 (1998) 193-201.
68. I.N. Kuznetsova, V. Blaskov, L. Znaidi, *Mater. Sci. Eng. B* 137 (2007) 31-39.
69. C.-S. Hsu, C.-K. Lin, C.-C. Chan, C.-C. Chang, C.-Y. Tsay, *Thin Solid Films* 494 (2006) 228-233.
70. H. Wang, C.C. Oey, A.B. Djurišić, K.K.Y. Man, W.K. Chan, M.H. Xie, Y.H. Leung, P.C. Chui, A. Pandey, J-M. Nunzi, *Proc. IEEE Conf. Nanotechnol.* Nagoya, Japan, July 2005
71. Y.-J. Kim, L.F. Francis, *J. Am. Ceram. Soc*. 76 (1993) 737-742.
72. L.H. Slooff, J.M. Kroon, J. Loos, M.M. Koetse, J. Sweelssen, *Adv. Funct. Mater*. 15 (2005) 689-694.
73. R. Könenkamp, P. Hoyer and A. Wahi. *J. Appl. Phys*. 79 (1996) 7029-7035.
74. C. Rost, S. Sieber, K. Ernst, S. Siebentritt, M.Ch. Lux-Steiner, R. Könenkamp. *Appl. Phys. Lett.* 75 (1999) 692-694.
75. A. Belaidi, R. Bayon, L. Dloczik, K. Ernst, M.Ch. Lux-Steiner, R. Könenkamp, *Thin Solid Films* 431-432 (2003) 488-491.

76. K. Ernst, A. Belaidi, R. Könenkamp, *Semicond. Sci. Technol*. 18 (2003) 475-479.
77. J. Wienke, M. Krunks, F. Lenzmann, *Semicond. Sci. Technol.* 18 (2003) 876-880.
78. M. Nanu, J. Schoonman, A. Goossens, *Nano Lett.* 5 (2005) 1716-1719.
79. R. O'Hayre, M. Nanu, J. Schoonman, A. Goossens, Q. Wang, M. Grätzel, *Adv. Funct. Mater.* 16 (2006) 1566-1576.
80. R. Bayon, R. Musembi, A. Belaidi, M. Bär, T. Guminskaya, M.Ch. Lux-Steiner, Th. Dittrich, *Sol. Energ. Mater. Sol. Cell.* 89 (2005) 13-25.
81. F. Lenzmann, M. Nanu, O. Kijatkina, A. Belaidi, *Thin Solid Films* 451-452 (2004) 639-643.
82. A. Mere, A. Katerski, O. Kijatkina, M. Krunks, 2004, *Proc. 19-th PVSEC*, June 7-11, 2004, Paris, 1973-1976.
83. K. Taretto, U. Rau, *Prog. Photovolt., Res. Appl*. 12 (2004) 573-591.
84. M. Fröba, O. Muth, A. Reller, *Solid State Ionics* 101-103 (1997) 249-253.
85. C.R. Hubbard, E.H. Evans, D. K. Smith, *J. Appl. Cryst*. 9 (1976) 169-174.
86. C. Suresh, V. Biju, P. Mukundan, K.G.K. Warrier, *Polyhedron* 17 (1998) 3131-3135.
87. S.K. Ghosh, A.K. Vasudevan, P.P. Rao, K.G.K. Warrier, *Br. Ceram. Trans*. 100 (2001) 151-154.
88. S. Riyas, P.N. Mohan Das, *Br. Ceram. Trans*. 103 (2004) 23-28.
89. J. Von Hoene, R.G. Charles, W.M. Hickam, *J. Phys. Chem*. 62 (1958) 1098-1101.
90. B.A. Tuttle, R.W. Schwartz, *MRS Bulletin*, June (1996) 49-54.
91. M. Toyoda, J. Watanabe, T. Matsumiya, *J. Sol-Gel Sci. Technol*. 16 (1999) 93-99.
92. Y. Djaoued, R. Taj, R. Brüning, S. Badilescu, P.V. Ashrit, G. Bader, T. Vo-Van, *J. Non-Cryst. Solids* 297 (2002) 55-56.
93. M. Burgos, M. Langlet, *Thin Solid Films* 349 (1999) 19-23.
94. O. Harizanov, A. Harizanova, *Sol. Energ. Mater. Sol. Cell.* 63 (2000) 185-195.
95. L. Miao, S. Tanemura, S. Toh, K. Kaneko, M. Tanemura, *J. Cryst. Growth* 264 (2004) 246-252.
96. S. Music, M. Gotic, M. Ivanda, S. Popovic, et al., Mater. *Mater. Sci. Eng. B, Solid-State Mater. Adv. Technol.* 47 (1997) 33-40.
97. J.C. Parker, R.W. Siegel, *J. Mater. Res*. 5 (1990) 1246-1252.
98. A. Turković, M. Ivanda, V. Vraneša, A. Drašner, *Vacuum*, 5-7 (1992) 471-473.
99. J. Aarik, A. Aidla, H. Mändar, V. Sammelselg, *J. Cryst. Growth* 220 (2000) 531-537.
100. N. Rausch, E.P. Burte, *J. Electrochem. Soc*. 140 (1993) 145-149.
101. S.K. Kim, W.-D Kim, K.-M. Kim, C.S. Hwang, J. Jeong, *Appl. Phys. Lett.* 85 (2004) 4112-4114.
102. N. Rausch, E. P. Burte, *Microel. Eng.* 19 (1992) 725-728.

103. H. Fukuda, S. Namioka, M. Miura, Y. Ishikawa, M. Yoshino, S. Nomura, *Jpn. J. Appl. Phys.* 38 (1999) 6034-6038.
104. H.K. Ha, M. Yoshimoto, H. Koinuma, B.-K. Moon, H. Ishiwara, *Appl. Phys. Lett*. 68 (1996) 2965-2967.
105. S.A. Campbell, D.C. Gilmer, X.-S. Wang, M.-T. Hsien, H.-S. Kim, W.L. Gladfelter, J. Yan, *IEE Trans. Electron. Dev.* 44 (1997) 104-109.
106. H. Fukuma, Y. Ishikawa, S. Namioka, *MRS Symp. Proc.* 606, Warrendale, PA, 2000, 106.
107. T.W. Kim, M. Jung, H.J. Kim, T.H. Park, Y.S. Yoon, W.N. Kang, S.S. Yom, *Appl. Phys. Lett*. 64 (1994) 1407-1409.
108. M. Kadoshima, M. Hiratani, Y. Shimamoto, K. Torii, H. Miki, S. Kimura, T. Nabatame, *Thin Solid Films*, 424 (2003) 224-228.
109. M.J. Alam, D.C. Cameron, *J. Sol-Gel Sci. Technol.* 25 (2002) 137-145.
110. D. Mardare, G.I. Rusu, *Mater. Sci. Eng. B, Solid-State Mater. Adv. Technol.* 75 (2000) 68-71.
111. H. Tang, K. Prasad, R. Sanjies, P.E. Schmid, F. Lévy, *J. Appl. Phys*. 75 (1994) 2042-2047.
112. T. Kanniainen, S. Lindroos, R. Resch, M. Leskelä, G. Friedbacher, M. Grasserbauer, *Mater. Res. Bull.* 35 (2000) 1045-1051.
113. S. Lindroos , T. Kanniainen, M. Leskelä, *Appl. Surf. Sci.* 75 (1994) 70-74.
114. T. Kanniainen, S. Lindroos, T. Prohaska, G. Friedbacher, M. Leskelä, M. Grasserbauer, L. Niinistö, *J. Mater. Chem.* 5 (1995) 985-989.

Appendix A

Article I

M. Krunks, **I. Oja**, K. Tõnsuaadu, M. Es-Souni, M. Gruselle, L. Niinistö, Thermoanalytical study of acetylacetonate-modified titanium(IV) isopropoxide as a precursor for TiO_2 films, *Journal of Thermal Analysis and Calorimetry*, 80 (2005) 483–488.

Appendix A

Article II

I. Oja Açik, J. Madarász, M. Krunks, K. Tõnsuaadu, J. Denke, G. Pokol, L. Niinistö, Thermoanalytical study of titanium(IV) acetylacetonate xerogels with emphasis on evolved gas analysis, *Journal of Thermal Analysis and Calorimetry*, 88 (2007) 2, in press (DOI:10.1007/s10973-006-8064-6).

Appendix A

Article III

I. Oja, A. Mere, M. Krunks, C.-H. Solterbeck, M. Es-Souni, Properties of TiO_2 films prepared by the spray pyrolysis method, *Solid State Phenomena*, 99-100 (2004) 259–262.

Appendix A

Article IV

I. Oja, A. Mere, M. Krunks, R. Nisumaa, C.-H. Solterbeck, M. Es-Souni, Structural and electrical characterization of TiO_2 films grown by spray pyrolysis, *Thin Solid Films,* 515 (2006) 674-677.

Appendix A

Article V

J. Sabataityte, **I. Oja**, F. Lenzmann, O. Volobujeva, M. Krunks, Characterization of nanoporous TiO_2 films prepared by sol-gel method. *Comptes Rendus Chimie*, 9 (2006) 708– 712.

Appendix A

Article VI

I. Oja, A. Belaidi, L. Dloczik, M.-Ch. Lux-Steiner, Th. Dittrich, Photoelectrical properties of $In(OH)_xS_y/PbS(O)$ structures deposited by SILAR on TiO_2. *Semiconductor Science and Technology*, 21 (2006) 520–526.

Appendix B

Curriculum Vitae

Appendix B

Curriculum vitae

Ees- ja perekonnanimi	Ilona Oja Açik
Sünniaeg ja –koht	17.11.1977 Eesti
E-post	ilona@staff.ttu.ee
Hariduskäik	2003-2007 Tallinna Tehnikaülikool, Keemia- ja materjalitehnolooga teaduskond, doktorantuur 2003- Tallinna Tehnikaülikool, Keemia- ja materjalitehnolooga teaduskond, loodusteaduste magistrikraad 2001- Tallinna Tehnikaülikool, Keemia- ja materjalitehnolooga teaduskond, loodusteaduste bakalaureusekraad 1996- Kärdla Keskkool, keskharidus
Teenistuskäik	2003- Tallinna Tehnikaülikool, Materjaliteaduse instituut, teadur 2002-2003 Tallinna Tehnikaülikool, Materjaliteaduse instituut, insener 1999-2001 Tallinna Tehnikaülikool, Materjaliteaduse instituut, tehniline töötaja
Kaitstud lõputööd	„TiO_2 õhukesed kiled sool-geel meetodil" magistritöö, juhendaja vanemteadur Malle Krunks „Pihustuspürolüüsi lähteainete ja pihustatud $CuInS_2$ õhukeste kilede uurimine infrapunase spektroskoopia meetodil", bakalaureusetöö, juhendaja vanemteadur Malle Krunks
Täiendõpe	aug.- sept. 2005 PV Interact, Berliin, Saksamaa veebr.- juuli 2005 Hahn-Meitner-Institut Berliin, Saksamaa, külalisteadur okt.- dets.2004 Vienna University of Technology, Austria, külalisteadur okt. 2003 Delft University of Technology, Holland, külalisteadur 2001- 2002 Kiel University of Applied Sciences, Saksamaa, külalisteadur juuni- aug. 2000 Chemnitz University of Technology, Saksamaa, praktikant juuli– aug. 1999 Queen's University, Belfast, Põhja-Iirimaa, praktikant

Appendix B

Curriculum vitae

First name and surname	Ilona Oja Açik
Date and place of birth	17.11.1977 Estonia
E-mail	ilona@staff.ttu.ee
Education	2003-2007 Tallinn University of Technology, Faculty of Chemical and Materials Technology, doctoral study 2003- Tallinn University of Technology, Faculty of Chemical and Materials Technology, Master of Science in Natural Sciences 2001- Tallinn University of Technology, Faculty of Chemical and Materials Technology, Bachelor of Science in Natural Sciences 1996- Kärdla Secondary School
Professional experience	2003- up to now Tallinn University of Technology, Department of Materials Science, researcher 2002- 2003 Tallinn University of Technology, Department of Materials Science, engineer 1999- 2001 Tallinn University of Technology, Department of Materials Science, technical assistant
Defended dissertations	„TiO_2 thin films by sol-gel process", master thesis, supervisor senior research scientist Malle Krunks ""Characterization of spray pyrolysis precursors and sprayed $CuInS_2$ thin films by IR spectroscopy"", bachelor thesis, supervisor senior research scientist Malle Krunks
Training courses	Aug.- Sept. 2005 PV Interact, Berlin, Germany Feb.- July 2005 Hahn-Meitner-Institut Berlin, Germany; guest researcher Oct.- Dec. 2004 Vienna University of Technology, Austria; guest researcher Oct. 2003 Delft University of Technology, The Netherlands; guest researcher 2001- 2002 Kiel University of Applied Sciences, Germany; guest researcher June- Aug. 2000 Chemnitz University of Technology, Germany; trainee July- Aug. 1999 Queen's University, Belfast, Northern Ireland; trainee

List of publications

1. I. Oja Açik, J. Madarász, M. Krunks, K. Tõnsuaadu, D. Jenke, G. Pokol, L. Niinistö, Thermoanalytical study of titanium(IV) acetylacetonate xerogels, *Journal of Thermal Analysis and Calorimetry*, 88 (2007) 2, in press (DOI:10.1007/s10973-006-8064-6).

2. M. Krunks, T. Dedova and I. Oja Açik, Spray pyrolysis deposition of zinc oxide nanostructured layers, *Thin Solid Films*, 515 (2006) 1157-1160.

3. I. Mora-Sero, J. Bisquert, F. Fabregat-Santiago, G. Garcia-Belmonte, G. Zoppi, K. Durose, Y. Proskuryakov, I. Oja, A. Belaidi, T. Dittrich, R. Tena-Zaera, A. Katty, C. Levy-Clement, V. Barrioz, S.J.C. Irvine, Implications of the Negative Capacitance Observed at Forward Bias in Nanocomposite and Polycrystalline Solar Cells, American Chemical Society*: Nano Letters.; (Letter),* 6 (2006) 640-650.

4. I. Oja, A. Belaidi, L. Dloczik, M.-Ch. Lux-Steiner and Th. Dittrich, Photoelectrical properties of $In(OH)_xS_y$/PbS(O) structures deposited by SILAR on TiO_2, *Semicond. Sci. Technol*., 21 (2006) 520-526.

5. S. Gavrilov, I. Oja, B. Lim, A. Belaidi, W. Bohne, E. Strub, J. Röhrich, M.-Ch. Lux-Steiner, Th. Dittrich, Charge selective contact on ultra-thin $In(OH)_xS_y$/$Pb(OH)_xS_y$ heterostructure prepared by SILAR. *Physica Status Solidi A- Applied Research*, 203 (2006) 1024-1029.

6. I. Oja, A. Mere, M. Krunks, R. Nisumaa, C.-H. Solterbeck, M. Es-Souni, Structural and electrical characterization of TiO_2 films grown by spray pyrolysis, *Thin Solid Films*, 515 (2006) 674-677.

7. J. Sabataityte, I. Oja, F. Lenzmann, O. Volobujeva, M. Krunks, Characterization of nanoporous TiO_2 films prepared by sol-gel method, *Comptes Rendus Chimie* 9 (2006) 708-712.

8. M. Krunks, I. Oja, K. Tõnsuaadu, M. Es-Souni, M. Gruselle and L. Niinistö, Thermoanalytical study of acetylacetonate-modified titanium(IV)isopropoxide as a precursor for TiO_2 films, *Journal of Thermal Analysis and Calorimetry*, 80 (2005) 483–488.

9. I. Oja, M. Nanu, A. Katerski, M. Krunks, A. Mere, J. Raudoja, A. Goossens, Crystal quality studies of $CuInS_2$ films prepared by spray pyrolysis, *Thin Solid Films*, 480-481 (2005) 82-86.

10. A. Jagomägi, J. Krustok, J. Raudoja, I. Oja, M. Grossberg, M. Krunks, Photoluminescence and raman spectroscopy of polycrystalline $AgInTe_2$, *Thin Solid Films*, 480-481 (2005) 246-249.

11. M. Krunks, O. Kijatkina, A. Mere, T. Varema, I. Oja, V. Mikli, Sprayed Large Grain $CuInS_2$ Films as Absorbers for Solar Sells, *Solar Energy Materials and Solar Cells*, 87 (2005) 207-214.

12. T. Dedova, M. Krunks, O. Volobujeva, I. Oja, ZnS thin films deposited by spray pyrolysis technique, *Physica Status Solidi c*, 2 (2005) 1161-1166.

13. T. Dedova, A. Mere, M. Krunks, O. Kijatkina, I. Oja, O. Volobujeva, Structural and optical characterization of sprayed ZnS thin films, in *Proceedings of SPIE* vol. 5946 *"Optical Materials and Applications", edited by Arnold Rosental,* (2005) 34-40.

14. I. Oja, A. Mere, M. Krunks, C.-H. Solterbeck, M. Es-Souni, Properties of TiO_2 films prepared by spray pyrolysis method, *Solid State Phenomena*, 99-100 (2004) 259-264.

15. M. Es-Souni, I. Oja, M. Krunks, Chemical Solution Deposition of Thin TiO_2-Anatase Films for Dielectric Applications, *Journal of Materials Science B: Materials in Electronics,* 15 (2004) 341-344.

16. P. Harvonen, T. Kaps, I. Oja, Chemical changes of the surface of the weathered wood, *Proceedings of Baltic Polymer Symposium 2003*, Jurmala, 17-19 Sept. 2003, RTU (2003) 244-248.

17. M. Krunks, O. Kijatkina, H. Rebane, I. Oja, V. Mikli, A. Mere, Composition of $CuInS_2$ thin films prepared by spray pyrolysis, *Thin Solid Films*, 403-404 (2002) 71-75.

18. M. Krunks, O. Kijatkina, J. Blums, I. Oja, A. Mere, E. Mellikov, Cost-effective sprayed $CuInS_2$ films for solar cells, *Proceedings 17-th EUPVSEC*, München 22-26 Oct. 2001, 2 (2002) 1211-1214.

Patent application:

1. Malle Krunks, Ilona Oja, Tatjana Dedova, Method of preparing zinc oxide nanorods on a substrate by chemical spray pyrolysis, international patent application WO2006/108425, (Priority No. US20050671232P, priority date 04/14/2005.).

DISSERTATIONS DEFENDED AT TALLINN UNIVERSITY OF TECHNOLOGY ON *NATURAL AND EXACT SCIENCES*

1. **Olav Kongas**. Nonlinear dynamics in modeling cardiac arrhytmias. 1998.

2. **Kalju Vanatalu**. Optimization of processes of microbial biosynthesis of isotopically labeled biomolecules and their complexes. 1999.

3. **Ahto Buldas**. An algebraic approach to the structure of graphs. 1999.

4. **Monika Drews**. A metabolic study of insect cells in batch and continuous culture: application of chemostat and turbidostat to the production of recombinant proteins. 1999.

5. **Eola Valdre**. Endothelial-specific regulation of vessel formation: role of receptor tyrosine kinases. 2000.

6. **Kalju Lott**. Doping and defect thermodynamic equilibrium in ZnS. 2000.

7. **Reet Koljak**. Novel fatty acid dioxygenases from the corals *Plexaura homomalla* and *Gersemia fruticosa.* 2001.

8. **Anne Paju**. Asymmetric oxidation of prochiral and racemic ketones by using sharpless catalyst. 2001.

9. **Marko Vendelin**. Cardiac mechanoenergetics *in silico*. 2001.

10. **Pearu Peterson**. Multi-soliton interactions and the inverse problem of wave crest. 2001.

11. **Anne Menert**. Microcalorimetry of anaerobic digestion. 2001.

12. **Toomas Tiivel**. The role of the mitochondrial outer membrane in *in vivo* regulation of respiration in normal heart and skeletal muscle cell. 2002.

13. **Olle Hints**. Ordovician scolecodonts of Estonia and neighbouring areas: taxonomy, distribution, palaeoecology, and application. 2002.

14. **Jaak Nõlvak**. Chitinozoan biostratigrapy in the Ordovician of Baltoscandia. 2002.

15. **Liivi Kluge**. On algebraic structure of pre-operad. 2002.

16. **Jaanus Lass**. Biosignal interpretation: Study of cardiac arrhytmias and electromagnetic field effects on human nervous system. 2002.

17. **Janek Peterson**. Synthesis, structural characterization and modification of PAMAM dendrimers. 2002.

18. **Merike Vaher**. Room temperature ionic liquids as background electrolyte additives in capillary electrophoresis. 2002.

19. **Valdek Mikli**. Electron microscopy and image analysis study of powdered hard-metal materials and optoelectronic thin films. 2003.

20. **Mart Viljus**. The microstructure and properties of fine-grained cermets. 2003.

21. **Signe Kask**. Identification and characterization of dairy-related *Lactobacillus.* 2003.

22. **Tiiu-Mai Laht**. Influence of microstructure of the curd on enzymatic and microbiological processes in Swiss-type cheese. 2003.

23. **Anne Kuusksalu**. 2–5A synthetase in the marine sponge *Geodia cydonium*. 2003.

24. **Sergei Bereznev**. Solar cells based on polycristalline copper-indium chalcogenides and conductive polymers. 2003.

25. **Kadri Kriis**. Asymmetric synthesis of C_2-symmetric bimorpholines and their application as chiral ligands in the transfer hydrogenation of aromatic ketones. 2004.

26. **Jekaterina Reut**. Polypyrrole coatings on conducting and insulating substracts. 2004.

27. **Sven Nõmm**. Realization and identification of discrete-time onlinear systems. 2004.

28. **Olga Kijatkina**. Deposition of copper indium disulphide films by chemical spray pyrolysis. 2004.

29. **Gert Tamberg**. On sampling operators defined by Rogosinski, Hann and Blackman windows. 2004.

30. **Monika Übner**. Interaction of humic substances with metal cations. 2004.

31. **Kaarel Adamberg**. Growth characteristics of non-starter lactic acid bacteria from cheese. 2004.

32. **Imre Vallikivi**. Lipase-catalysed reactions of prostaglandins. 2004.

33. **Merike Peld**. Substituted apatites as sorbents for heavy metals. 2005.

34. **Vitali Syritski**. Study of synthesis and redox switching of polypyrrole and poly(3,4-ethylenedioxythiophene) by using *in-situ* techniques. 2004.

35. **Lee Põllumaa**. Evaluation of ecotoxicological effects related to oil shale industry. 2004.

36. **Riina Aav**. Synthesis of 9,11-secosterols intermediates. 2005.

37. **Andres Braunbrück**. Wave interaction in weakly inhomogeneous materials. 2005.

38. **Robert Kitt**. Generalised scale-invariance in financial time series. 2005.

39. **Juss Pavelson**. Mesoscale physical processes and the related impact on the summer nutrient fields and phytoplankton blooms in the western Gulf of Finland. 2005.

40. **Olari Ilison**. Solitons and solitary waves in media with higher order dispersive and nonlinear effects. 2005.

41. **Maksim Säkki**. Intermittency and long-range structurization of heart rate. 2005.

42. **Enli Kiipli**. Modelling seawater chemistry of the East Baltic Basin in the late Ordovician–Early Silurian. 2005.

43. **Igor Golovtsov**. Modification of conductive properties and processability of polyparaphenylene, polypyrrole and polyaniline. 2005.

44. **Katrin Laos**. Interaction between furcellaran and the globular proteins (bovine serum albumin β–lactoglobulin). 2005.

45. **Arvo Mere**. Structural and electrical properties of spray deposited copper indium disulphide films for solar cells. 2006.

46. **Sille Ehala**. Development and application of various on- and off-line analytical methods for the analysis of bioactive compounds. 2006.

47. **Maria Kulp**. Capillary electrophoretic monitoring of biochemical reaction kinetics. 2006.

48. **Anu Aaspõllu.** Proteinases from *Vipera lebetina* snake venom affecting hemostasis. 2006.

49. **Lyudmila Chekulayeva**. Photosensitized inactivation of tumor cells by porphyrins and chlorins. 2006.

50. **Merle Uudsemaa**. Quantum-chemical modeling of solvated first row transition metal ions. 2006.

51. **Tagli Pitsi**. Nutrition situation of pre-school children in Estonia from 1995 to 2004. 2006.

52. **Angela Ivask**. Luminescent recombinant sensor bacteria for the analysis of bioavailable heavy metals. 2006.

53. **Tiina Lõugas**. Study on physico-chemical properties and some bioactive compounds of sea buckthorn (*Hippophae rhamnoides* L.). 2006.

54. **Kaja Kasemets**. Effect of changing environmental conditions on the fermentative growth of Saccharomyces cerevisae S288C: auxo-accelerostat study. 2006.

55. **Ildar Nisamedtinov**. Application of ^{13}C and fluorescence labeling in metabolic studies of Saccharomyces spp. 2006.

56. **Alar Leibak**. On additive generalisation of Voronoï's theory of perfect forms over algebraic number fields. 2006.

57. **Andri Jagomägi**. Photoluminescence of chalcopyrite tellurides.2006.

58. **Tõnu Martma**. Application of carbon isotopes to the study of the Ordovician and Silurian of the Baltic. 2006.

59. **Marit Kauk**. Chemical composition of $CuInSe_2$ monograin powders for solar cell application. 2006.

60. **Julia Kois**. Electrochemical deposition of $CuInSe_2$ thin films for photovoltaic applications. 2006.